

NASA/TM-2012-217754



Characterization of HIRF Susceptibility Threshold for a Prototype Implementation of an Onboard Data Network

*Wilfredo Torres-Pomales
Langley Research Center, Hampton, Virginia*

August 2012

NASA STI Program . . . in Profile

Since its founding, NASA has been dedicated to the advancement of aeronautics and space science. The NASA scientific and technical information (STI) program plays a key part in helping NASA maintain this important role.

The NASA STI program operates under the auspices of the Agency Chief Information Officer. It collects, organizes, provides for archiving, and disseminates NASA's STI. The NASA STI program provides access to the NASA Aeronautics and Space Database and its public interface, the NASA Technical Report Server, thus providing one of the largest collections of aeronautical and space science STI in the world. Results are published in both non-NASA channels and by NASA in the NASA STI Report Series, which includes the following report types:

- **TECHNICAL PUBLICATION.** Reports of completed research or a major significant phase of research that present the results of NASA Programs and include extensive data or theoretical analysis. Includes compilations of significant scientific and technical data and information deemed to be of continuing reference value. NASA counterpart of peer-reviewed formal professional papers, but having less stringent limitations on manuscript length and extent of graphic presentations.
- **TECHNICAL MEMORANDUM.** Scientific and technical findings that are preliminary or of specialized interest, e.g., quick release reports, working papers, and bibliographies that contain minimal annotation. Does not contain extensive analysis.
- **CONTRACTOR REPORT.** Scientific and technical findings by NASA-sponsored contractors and grantees.

- **CONFERENCE PUBLICATION.** Collected papers from scientific and technical conferences, symposia, seminars, or other meetings sponsored or co-sponsored by NASA.
- **SPECIAL PUBLICATION.** Scientific, technical, or historical information from NASA programs, projects, and missions, often concerned with subjects having substantial public interest.
- **TECHNICAL TRANSLATION.** English-language translations of foreign scientific and technical material pertinent to NASA's mission.

Specialized services also include organizing and publishing research results, distributing specialized research announcements and feeds, providing information desk and personal search support, and enabling data exchange services.

For more information about the NASA STI program, see the following:

- Access the NASA STI program home page at <http://www.sti.nasa.gov>
- E-mail your question to help@sti.nasa.gov
- Fax your question to the NASA STI Information Desk at 443-757-5803
- Phone the NASA STI Information Desk at 443-757-5802
- Write to:
STI Information Desk
NASA Center for AeroSpace Information
7115 Standard Drive
Hanover, MD 21076-1320

NASA/TM-2012-217754



Characterization of HIRF Susceptibility Threshold for a Prototype Implementation of an Onboard Data Network

*Wilfredo Torres-Pomales
Langley Research Center, Hampton, Virginia*

National Aeronautics and
Space Administration

Langley Research Center
Hampton, Virginia 23681-2199

August 2012

Acknowledgments

The author is grateful for the contributions to the work described here by the following individuals: Sandra V. Koppen, Mahyar M. Malekpour, Paul S. Miner, Celeste M. Belcastro, Eric G. Cooper, Jay J. Ely, Dr. Oscar R. Gonzalez, Dr. W. Steven Gray, John J. Mielnik, Jr., Truong X. Nguyen, Maria Theresa Salud, and Laura J. Smith.

Available from:

NASA Center for AeroSpace Information
7115 Standard Drive
Hanover, MD 21076-1320
443-757-5802

Abstract

An experiment was conducted to characterize the effects of HIRF-induced upsets on a prototype onboard data network. The experiment was conducted at the NASA Langley Research Center's High Intensity Radiation Field Laboratory and used a generic distributed system prototyping platform to realize the data network. This report presents the results of the hardware susceptibility threshold characterization which examined the dependence of measured susceptibility on factors like the frequency and modulation of the radiation, layout of the physical nodes and position of the nodes in the test chamber. The report also includes lessons learned during the development and execution of the experiment.

Table of Contents

1. Introduction	1
2. HSTC Background	3
3. HSTC Description	9
4. Results and Analysis.....	15
4.1. Power Cable Routing.....	15
4.2. Modulation	16
4.3. Physical Nodes	18
4.4. Chamber Positions	22
5. Final Remarks.....	24
Appendix A. Test Data.....	26
References	38
Acronyms	40

1. Introduction

An experiment was conducted to characterize the effects of a HIRF (High Intensity Radiated electromagnetic Field) environment on a prototype of an onboard data network [1, 2, 3]. This network provides the capabilities needed to develop processing architectures satisfying a wide range of application performance and dependability requirements, including Integrated Modular Architectures (IMA) [4] for safety-critical real-time applications [5, 6, 7, 8]. A distributed system architecture for those applications must have the ability to mitigate the effects of internal component faults of varying severity [9]. The potential of HIRF environments to generate severe fault conditions in electronic systems [10, 11] was leveraged in this physical fault injection experiment [12, 13] to examine the network's fault response. The experiment was divided in two parts. The HIRF Susceptibility Threshold Characterization (**HSTC**) was intended to examine factors that determine the minimum HIRF field strength level at which a particular electronic System Under Test (SUT) begins to experience HIRF-induced interference to its internal operation. The results and lessons learned in HSTC were used to finalize the specification of the second part of the experiment. The HIRF Effects Characterization (**HEC**) was intended to assess the system response to functional system **upsets** (i.e., functional error modes which involve no component damage and can occur simultaneously in all channels of a redundant system [14]) over a range of severity levels. This report documents the results of the HSTC part of the experiment. The results of the HEC will appear in future reports.

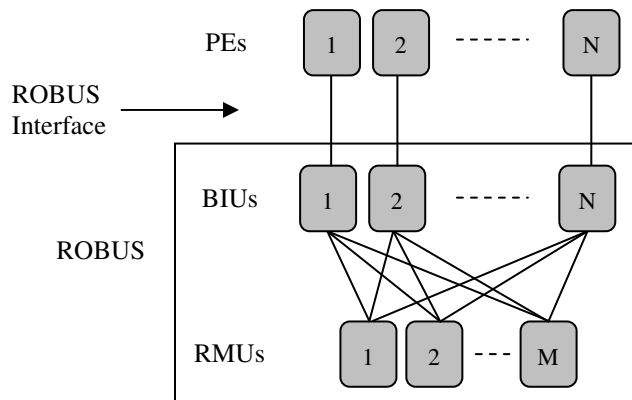


Figure 1: ROBUS-2 topology

The data network used in this experiment was ROBUS-2 [15, 16]. Figure 1 shows the ROBUS-2 topology. The network has a redundant active-star architecture with the Bus Interface Units (BIUs) serving as the access ports, and the Redundancy Management Units (RMUs) providing connectivity as network hubs. The network between BIUs and RMUs forms a complete bipartite graph in which each node is directly connected to every node of the opposite kind. All the communication links are bidirectional. At the interface to the PEs, ROBUS-2 behaves as a shared-medium communication bus with a TDMA (Time-Division Multiple Access) channel access pattern. ROBUS-2 was designed to be implemented as a set of custom hardware-level protocol processors performing ROBUS-2-specific functions hosted on a hardware platform providing basic communication resources at the physical layer. The design of the protocol processors is described in the VHDL language [17, 18] and can be realized either on an FPGA (Field-Programmable Gate Array chip) or an ASIC (Application-Specific Integrated Circuit). For this experiment, ROBUS-2 was implemented on the Reconfigurable SPIDER Prototyping Platform (RSPP), which is a general-purpose prototyping platform for distributed systems consisting of

FPGA-based nodes and fiber-optic communication links. Additional information about the physical prototyping platform is given in reports [1] and [2].

The experiment was conducted at the NASA Langley Research Center's High Intensity Radiated Fields (HIRF) Laboratory using reverberation chamber A of the facility to generate the HIRF environment [1]. Similar to a large microwave oven, the reverberation chamber operates as a cavity resonator in which the electric field generated by a transmitting antenna reflects off the metal walls forming complex three-dimensional electromagnetic field patterns with low energy loss. Rotating mechanical stirrers in the chamber effectively change the boundary conditions (i.e., spatial orientation of the reflective surfaces) in time, thus creating a time-varying field pattern that mixes the energy and produces a statistically uniform and isotropic HIRF environment. Figure 2 shows the inside of the chamber with the positions where the prototyping platform nodes could be placed on either non-conductive foam blocks or tables.



Figure 2: Reverberation chamber A with non-conductive foam blocks and tables

The purpose of HEC part of the experiment was to collect data on the response of the ROBUS-2 function to physical faults occurring on the prototyping platform caused by electromagnetic interference in the HIRF environment inside the reverberation chamber. Multiple configurations were tested to enable comparative analysis of HIRF responses [1]. To support the HEC, the HSTC part of the experiment was designed to examine how the field-strength susceptibility threshold of the prototyping nodes depends on the physical layout of the nodes, the frequency of the input signal driving the chamber's transmitting antenna, the input signal modulation, which specific physical node is being radiated, the particular ROBUS-2 function hosted by a node and the position of a node in the chamber. The data collected during HSTC was used to specify the physical layout of a node, to specify the HIRF strength, frequency and modulation test points, and to rank the physical nodes by their average susceptibility thresholds and the chamber positions by their average field strengths. These node and position rankings were then used to assign ROBUS-2 functions to nodes and nodes to chamber positions in HEC in order to reasonably match

the susceptibility thresholds of the various test configurations and thus reduce any possible biases in the HEC comparative response analyses due to differences in susceptibility thresholds among the tested configurations. The HSTC data was also used to specify how to scan the field strength and frequency during HEC tests to efficiently find upset susceptibility regions and minimize the likelihood of damaging the physical nodes from excessive radiated field coupling.

The report is organized as follows. The next section gives an overview and insight into how the specification of HSTC changed over time until it reached its final form presented in report [1] as we learned about the implications of the chamber radiation parameters and the node layout on the susceptibility threshold and response of the physical nodes. This is followed by a description of the HSTC objectives we settled on and the methodology used to achieve these objectives. Then the HSTC results and analysis are presented. The report ends with a summary and concluding remarks on the HSTC part of the experiment. The appendix shows the susceptibility threshold data collected in HSTC.

2. HSTC Background

The purpose of the HSTC was to determine how to generate HIRF-induced upsets in the nodes of the prototyping platform. This section describes how the HSTC evolved from its initial form developed based on vague notions of the HIRF chamber field dynamics and the interaction of the field with electronic devices, to its final form shaped by lessons learned through experimentation and careful analysis of observations. The knowledge and experience gained in the development of the HSTC strongly influenced not only the design of the HEC, but also the experiment design for a later project on the effects of HIRF on a distributed flight control system [19, 20, 21].

Our initial attempts to design a procedure to characterize the susceptibility threshold of the platform nodes leveraged existing descriptions of a mode-stirring reverberation chamber in which the field is isotropic, randomly polarized and uniform throughout the chamber. Essentially, we thought of the HIRF field in a mode-stirred reverberation chamber as being similar to random noise whose amplitude and central frequency could be easily controlled by changing the parameters of the input signal to the transmitting antenna. Additionally, based on the guidelines in the RTCA/DO-160D standard [22] and considering that the platform nodes were going to be tested with open enclosures (see Figure 3), it was thought that a field strength of no more 100 V/m and 25 geometrically spaced discrete frequencies over the range from 100 MHz to 1000 MHz would produce an adequate number of upset regions.

Initially we focused our effort in defining field amplitude modulation patterns with timing parameters derived from the analysis of the design of ROBUS-2. ROBUS-2 uses a full-system re-initialization strategy that is dependent on the assumption that the duration of external disturbances experienced by the system will be within an assumed maximum bound and that enough time will elapse between disturbances to allow the system to return to normal operation. There is no such assumption for scenarios in which a subset of nodes is affected by an external disturbance but the system remains operational in a degraded state. Thus, the experiment was viewed as a series of random-fault injection tests with the radiated field as the means of injecting faults. Each test of a hardware configuration was to be composed of a set of field exposures called **rounds**. Figure 4 illustrates the composition of a round. Each round consisted of a series of periodic radiation bursts called **strikes**, each of which was followed by a non-radiation idle interval called a **lull** in which the radiated device was allowed to recover and return to normal operation. In general, each strike was composed of one or more radiation pulses called **strokes**.

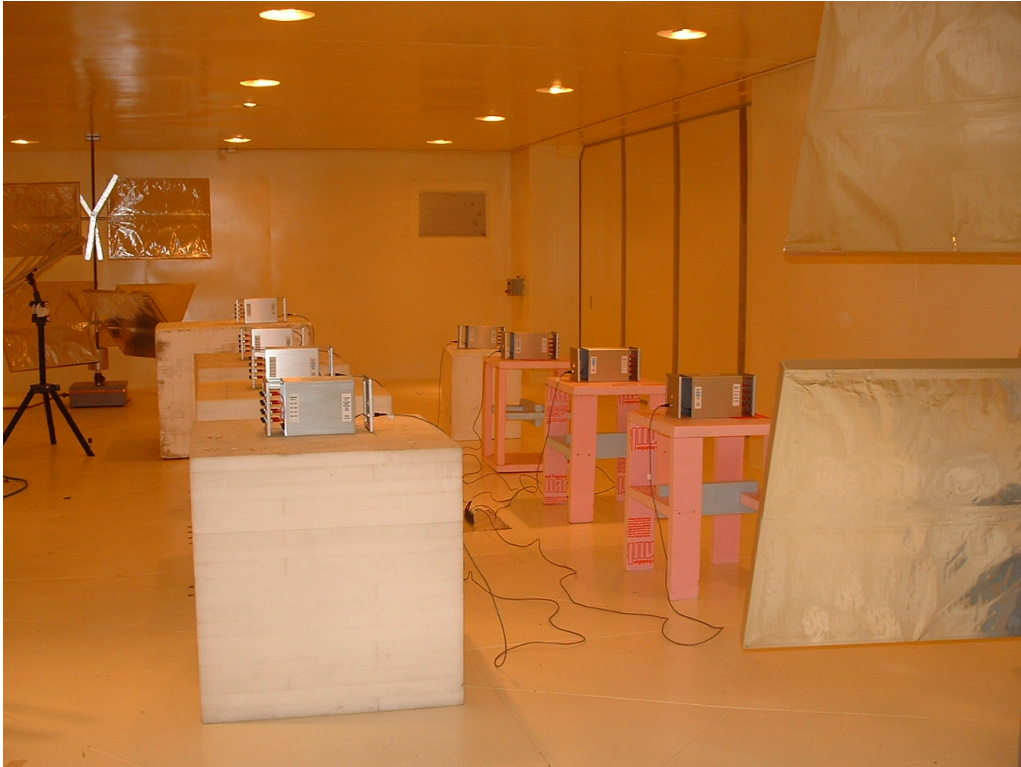


Figure 3: Nodes in chamber A with the shielding enclosures open (optical fibers not shown)

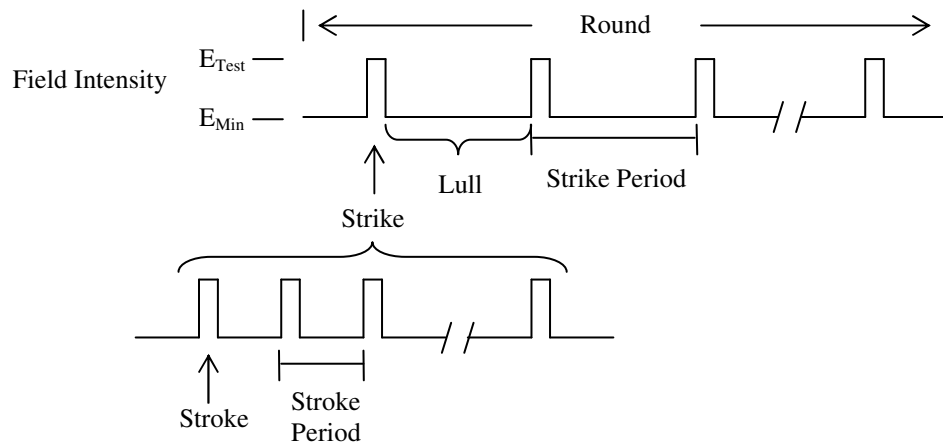


Figure 4: Radiation time pattern for a test round in the initial version of the experiment

The strokes were generated with a 1 KHz pulse modulation with a 90% depth and a pulse width of 20 μs (i.e., large enough to accommodate the chamber time constant which measures the rate at which the field amplitude increases in the chamber in response to a step increase in the input signal amplitude). A series of strike patterns were defined with variations in the duration of the strikes (which determines the number of strokes), the strike period, and the number of strikes in a round. To test the robustness of

ROBUS-2, the duration of the strikes were chosen to be either smaller or larger than the disturbance duration bound assumed in the design of ROBUS-2 (i.e., 150 ms). The strike periods were chosen to be larger than the expected worst-case recovery delay of ROBUS-2 (i.e., 2.15 seconds for individual node recovery and 4.18 seconds for full-system recovery) to ensure that each upset event could be handled in the analysis as an independent trial in a fault injection experiment. The actual strike periods were selected not to have a common divisor (i.e., were prime) relative to the duration of a stirrer rotation (i.e., 5 seconds) such that the stirrers would be at a different position for each strike. The durations of the rounds were chosen to have a large enough number of upsets for a meaningful statistical analysis of system fault response. Round durations of up to 205 seconds (i.e., 3.4 minutes) were tested. The stirrers were set to rotate at 5 seconds per revolution. The field strength and frequency test matrix was covered by first setting the desired field amplitude and varying the frequency over the whole range, then stepping up the field strength by 22.5 V/m and repeating the frequency sweep. One round was completed at each field strength and frequency test point, and every frequency was tested at every field strength level. At the time, it was assumed that the upset susceptibility threshold at a particular frequency was triggered by the field strength exceeding the immunity level of the most susceptible node components and that increasing the field strength beyond this level would trigger the failure of additional components and generate more complex (and interesting) node failure modes. Initially it was also assumed that all the nodes would have approximately the same susceptibility threshold profile over the frequency range because they are all physical replicas. Unfortunately, no upsets were observed with this initial setup with one node in the chamber at a predetermined position (i.e., node 4 at position 4).

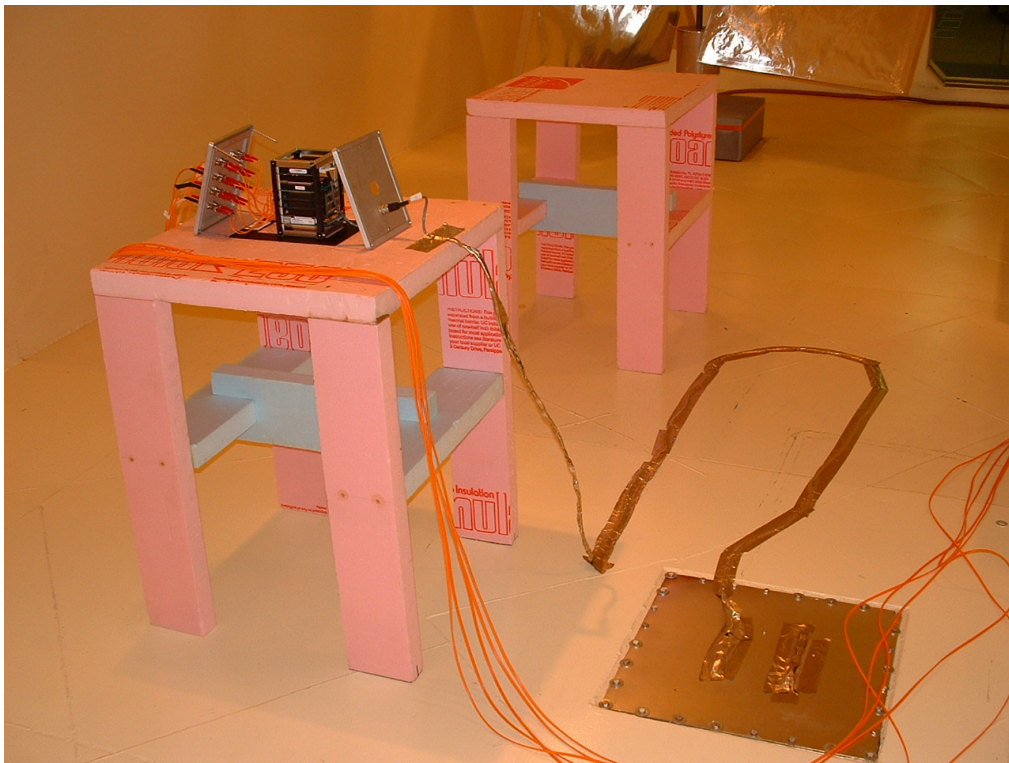


Figure 5: Layout of a node with the shielding enclosure removed

The failure of the first experimental setup led to a process of trial-and-error exploration to find a reliable way to produce upsets. The first change was to completely remove the enclosures from the nodes to allow the electromagnetic field to directly reach the electronic components. The basic layout of a node with this change is illustrated in Figure 5. This proved not to be enough to generate upsets even after

testing at every frequency and increasing the maximum field strength to 120 V/m. So the decision was made to continue increasing the field strength in steps of 20 V/m in an attempt to “calibrate” the test parameters by identifying the field-strength upset level at each frequency. Because it was noticed that the measured susceptibility threshold at a particular frequency sometimes was different when retesting for it, it was decided that after an upset occurred at a particular field strength, the same frequency would be tested at a higher field strength to confirm that a repeatable condition had been reached. A frequency was removed from the test set only after confirmation of the upset threshold. Table 1 shows the results of this test for node 4 at position 4. This test was followed by another test at 618.97 MHz that consisted of running 10 rounds at 0, 20 and 40 V/m above the calibrated susceptibility threshold in order to confirm that the measured result was repeatable and that the node would indeed fail every time it was exposed to a field strength higher than the measured threshold. A positive result in this test lead us to believe that we had found a reliable way to generate upsets.

Using the field-strength susceptibility profile in Table 1, a series of single-radiated-node tests were conducted in which rounds were executed at 0, 40 and 80 V/m above the calibrated threshold for each test frequency with a known susceptibility threshold. Although we were able to complete many rounds using different strike patterns, the radiated nodes experienced a large number of permanent component failures at an increasing rate. The failed components included in-stack power supplies, fan boards, CPUs, and FPGA boards. Figure 6 shows a power supply board which failed at 40 V/m above the susceptibility threshold. Notice the charred area indicative of overheating near the center of the board. While executing these rounds, it was noticed on the display of the AC-to-DC power supply in the Control Room (which powered the radiated node in the chamber) that the current supplied to the node was slowly increasing as the radiation exposure continued. This was interpreted as an indication that the in-stack power supply at the radiated node was experiencing a cumulative overstress failure mode. At that point, it was realized that, considering how quickly we were losing parts, we would not be able to complete a meaningful experiment before running out of spares and, more importantly, that most of the observed upsets were probably due to power supply degradation rather than interference effects on the logic components of the nodes.

Table 1: Susceptibility thresholds measured during upset-level calibration test with explicit strike pattern

Field Frequency (MHz)	Susceptibility Threshold (V/m)	Field Frequency (MHz)	Susceptibility Threshold (V/m)
100	320	348.07	560
110.07	340	383.12	200
121.15	380	421.7	160
133.35	300	464.16	540
146.78	380	510.9	Larger than 800
161.56	180	562.34	780
177.83	360	618.97	620
195.73	280	681.29	Larger than 800
215.44	Larger than 800	749.89	Larger than 800
237.14	Larger than 800	825.4	Larger than 800
261.02	Larger than 800	908.52	500
287.3	Larger than 800	1000	Larger than 800
316.23	800	--	--

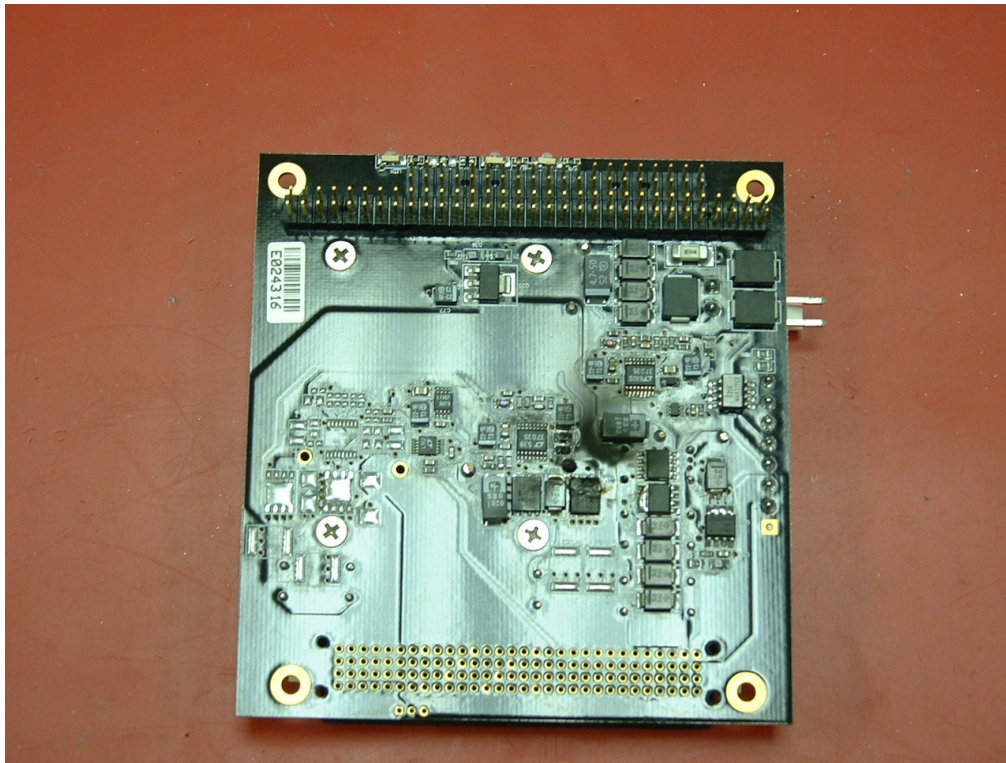


Figure 6: Power supply board that failed at 40 V/m above the susceptibility threshold

This situation lead us to reduce the number of strikes per round by 80% without changing the strike duration in order to reduce the total radiation exposure. This was implemented by increasing the period between strikes to allow additional time for the node's power supply to stabilize between radiation bursts. However, this change was ineffective in reducing the rate of power supply failures as they continued to happen unabated.

The next change tried was to replace the in-stack power supply from a 50 W rating to a 75 W rating to test a hypothesis that a more powerful device would also be more robust relative to HIRF radiation. This was quickly proved false as two 75 W power supplies failed in quick succession.

We also tried moving the node to a different position in the chamber, but this change was also shown ineffective as the health monitoring system [2] located in the Control Room recorded a massive series of errors from the radiated node. Although the node's components had not failed permanently, the volume of errors was viewed as an indication that the node was overwhelmed by the strength of the radiation and that continued exposure would quickly lead to a permanent failure. At this point, the experiment was suspended indefinitely until a new approach could be developed to generate logic upsets without causing permanent damage to the prototyping platform.

Various observations were taken into consideration in the redesign of the experiment. A critical observation was that the most susceptible node component was the in-stack power supply and that although its design enabled it to absorb radiation for a long time with minimal effect at its output, eventually the total radiation exposure would cause it to fail permanently. It was assumed that a high field strength would accelerate the failure of the power supply.

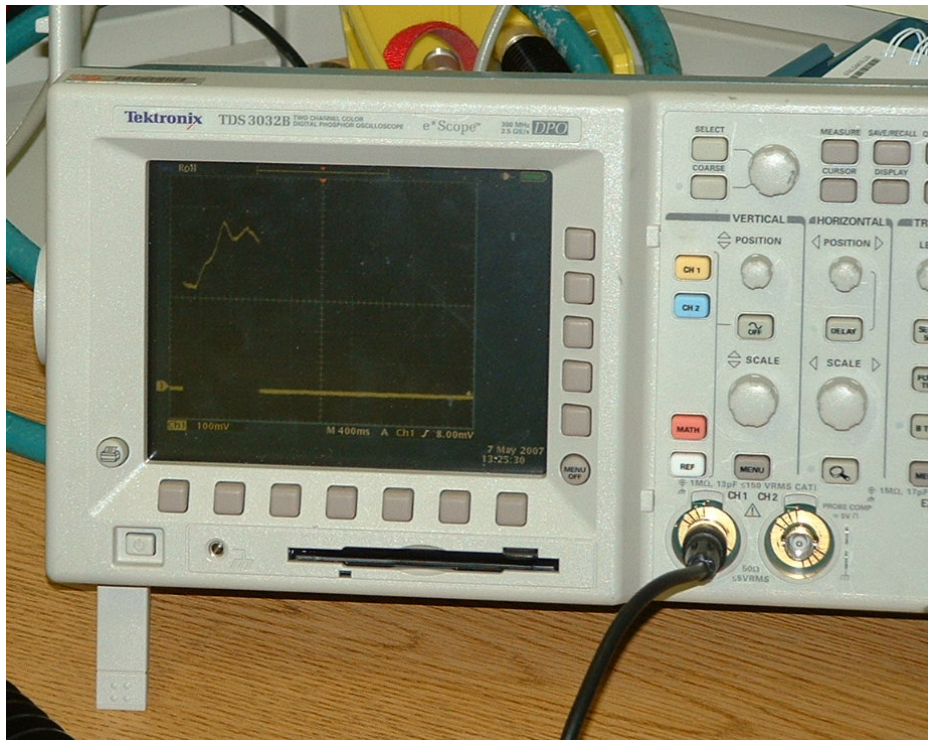


Figure 7: Peak field amplitude during a strike measured at the output of the receive antenna in the chamber

Figure 7 illustrates a casual observation that turned out to be one of the most significant insights into the operation of the reverberation chamber and eventually lead to the successful redesign of the experiment. This figure shows an oscilloscope trace of the peak field strength amplitude during a strike measured at the output of the receive antenna which is located inside the reverberation chamber. Notice how the amplitude varies in time and recall that the field stirrers in the chamber were constantly rotating during a round. In the particular round during which this measurement was made, the strikes had a duration of 100 ms and the stirrers had a revolution period of 5 seconds. Therefore, the shown peak field-amplitude trace covers only a small fraction of a stirrer’s revolution. Contrary to what had been assumed, the peak field strength at a position in the chamber during a strike was not constant in time but a function of the angular position of the stirrers. From this it was deduced that this time varying stirrer-induced field-strength-amplitude modulation (SIM) was how the stirrers made the field uniform (in a statistical sampling sense) throughout the chamber. Therefore, in effect, our pulse-based strike pattern was sampling this SIM waveform, and based on the large SIM amplitude variation seen in Figure 7, the nodes were being exposed to radiation bursts of widely varying and essentially random field strengths. This would help explain, in part, why repeatability of test results was so poor and why we saw so many long sequences of testing with no observed effects even after increasing the nominal severity of the HIRF environment.

The HSTC approach described in the next section incorporated the lessons learned from this initial attempt to define a safe and reliable methodology to generate HIRF-induced upsets.

3. HSTC Description

The purpose of the HSTC was to characterize the dependence of the HIRF susceptibility threshold of the prototyping platform nodes to variations in the field frequency, modulation, physical layout of the nodes, individual nodes, and positions in the chamber. To account for possible irremediable differences in the susceptibility thresholds of the nodes or the relative strength of the field at the various test positions in the chamber, the data collected in the HSTC had to support an analysis to rank the nodes by their immunity to HIRF and the positions by the severity of their local environments. Table 2 on page 13 of report [2] shows the planned test sequence for the HSTC. Table 3 below shows the actual tests performed. Figures 8 and 9 illustrate the test setups for HSTC configurations HC3 and HC4. These 4x4 ROBUS-2 configurations with a single node in the chamber were selected for the HSTC for several reasons: (1) the theory of design of ROBUS-2 guaranteed that the nodes outside the chamber were immune to errors generated by the radiated node and they would preserve coordinated, error-free and highly deterministic operation in the value and time domains regardless of any behavior exhibited by the radiated node; (2) by virtue of their immunity to error from the radiated node, the nodes outside the chamber provided a stable message traffic environment that enabled efficient error recovery by the radiated node; (3) the low data transfer rate allowed the nodes to operate with non-overlapping reception windows, which increased the input error detection coverage (see Section 5 of report [2]); and (4) because there was a single node in the chamber, it was known that any observed errors originated from faults occurring at the radiated node. These conditions greatly simplified the analysis of HSTC results. Basically, any error reported by any of the System Health Monitors at either the PE Emulator or the Bus Monitor (see reports [1] and [2]) signaled that the radiated node was being exposed to a field strength at or above its susceptibility threshold.

The field stirrers were set to rotate at 10 seconds per revolution and each test round lasted for 30 seconds (i.e. 3 stirrer revolutions) at a particular field strength and frequency point. The relatively slow stirrer speed was meant to slow down the rate of change of the SIM waveform and enable longer exposure of the node to every part the SIM. The round duration was set large enough to allow the node to be exposed to a few passes of the SIM.

A 2-out-of-3 rule was used to confirm an observed susceptibility threshold. This rule required that a susceptibility threshold observed during a round at a particular field strength and frequency had to be confirmed by repeating the round a total of at most three times and observing the susceptibility in two of the rounds. Report [1] describes this rule and its implementation in detail.

Table 3: Actual HSTC tests performed

HSTC Test Id	Hardware Configuration	Variable of Interest	Functional ROBUS Node	Physical RSPP node	Chamber Position	Modulation	Field Strength (V/m)
1	HC3	Physical Node	RMU 1	5	5	CW	20 - 300
2	HC4	Physical Node	BIU 1	1	5	CW	20 - 300
3	HC4	Physical Node	BIU 1	2	5	CW	20 - 300
4	HC4	Physical Node	BIU 1	3	5	CW	20 - 300
5	HC4	Physical Node	BIU 1	4	5	CW	20 - 300
6	HC3	Physical Node	RMU 1	6	5	CW	20 to 300
7	HC3	Physical Node	RMU 1	7	5	CW	20 - 300
8	HC3	Physical Node	RMU 1	8	5	CW	20 - 300
9	HC3	Modulation	RMU 1	5	5	Pulse	20 - 500
10	HC4	Position	BIU 1	1	1	CW	20 - 300
11	HC4	Position	BIU 1	2	2	CW	20 - 300
12	HC4	Position	BIU 1	3	3	CW	20 - 300
13	HC4	Position	BIU 1	4	4	CW	20 - 300
14	HC3	Position	RMU 1	6	6	CW	20 - 300
15	HC3	Position	RMU 1	7	7	CW	20 - 300
16	HC3	Position	RMU 1	8	8	CW	20 - 300
17	HC3	Modulation	RMU 1	5	5	Square wave	20 - 400
18	HC3	Power Cable Routing 1	RMU1	8	5	CW	20 - 300
19	HC3	Power Cable Routing 2	RMU1	8	5	CW	20 - 300
20	HC3	Power Cable Routing 3	RMU1	8	5	CW	20 - 300
21	HC3	Power Cable Routing 4	RMU1	8	5	CW	20 - 300
22	HC3	Power Cable Routing 2	RMU1	7	5	CW	20 - 300

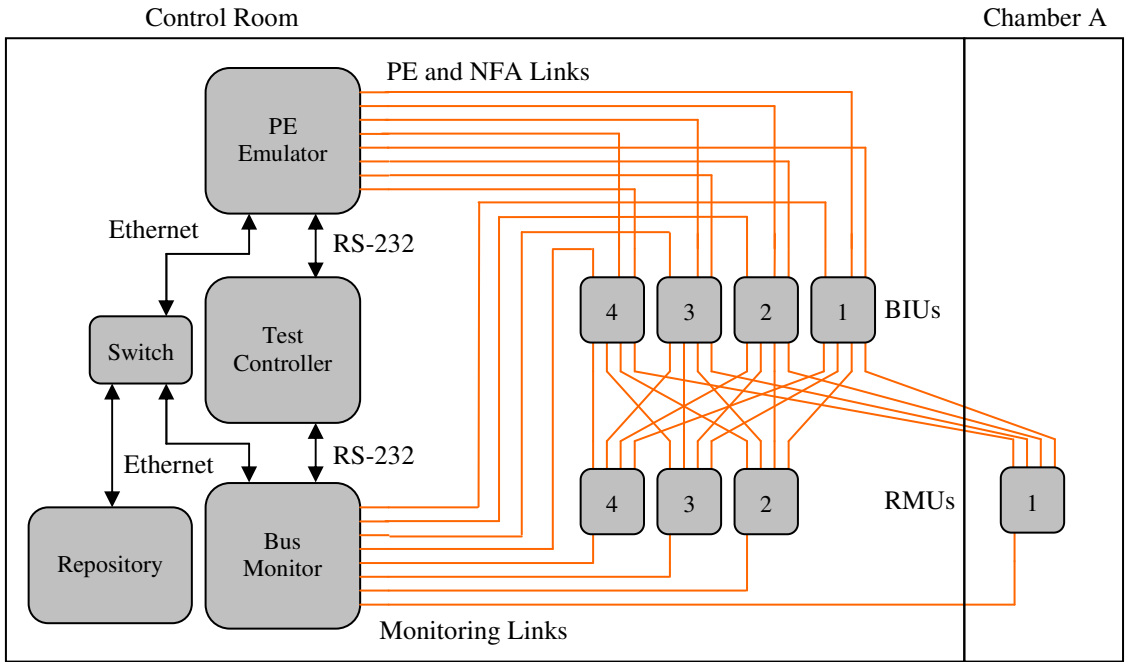


Figure 8: Test setup for hardware configuration HC3

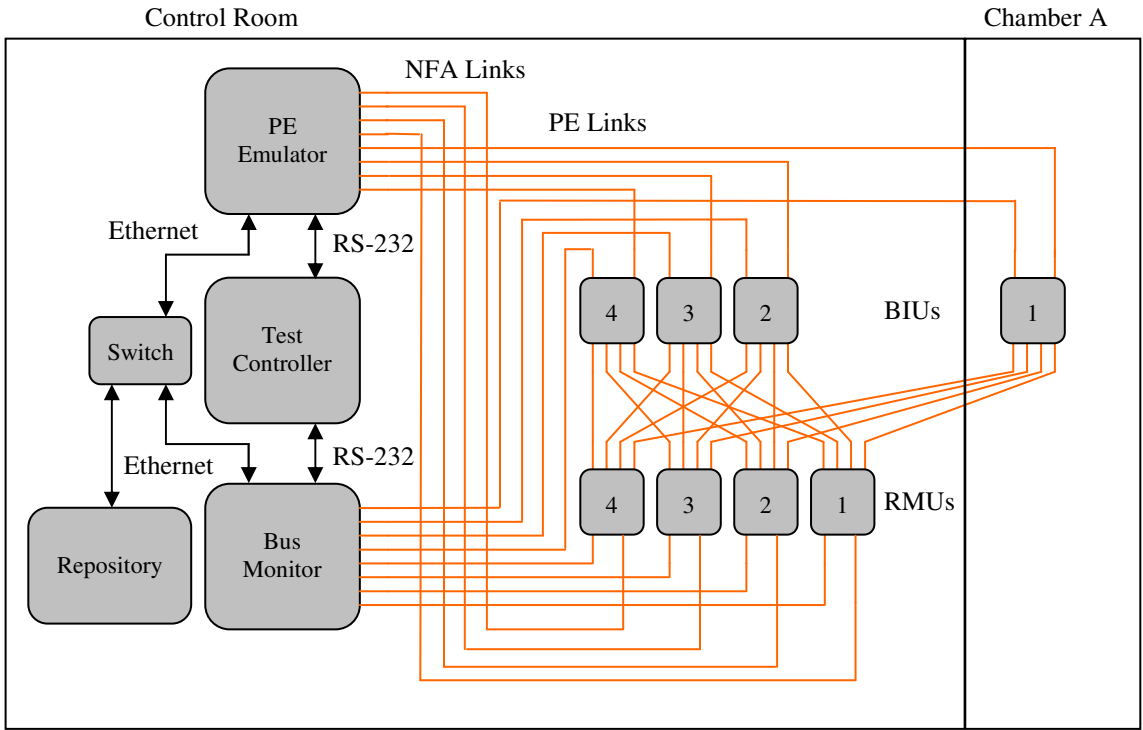


Figure 9: Test setup for hardware configuration HC4

Tests 1, 9, and 17 were intended to allow a comparative analysis of the effects of the transmit antenna's input signal modulation on the susceptibility threshold of a node. Notice that the maximum field strength was 300 V/m for CW (no modulation), 400 V/m for square wave modulation (1 kHz with 50% duty cycle), and 500 V/m for pulse modulation (20 μ s pulses at a rate of 1 kHz). This increase in maximum field strength was driven by the opposite trend of decreasing SIM waveform sampling coverage achieved by the specified modulation patterns. CW achieves 100% coverage of the SIM waveform, the square waveform modulation achieves at least 50% coverage, and the pulse modulation achieves at least 2% coverage. (The coverage is higher than the duty cycle if the stirrer revolution period is not a multiple of the modulation period.) Unless the round duration is made larger in order to increase the number of SIM samples per round, a decrease in SIM coverage implies an uncertainty increase in the ability to measure the susceptibility threshold of a node. The increase in maximum field strength was intended to accommodate a chance scenario in which the node is exposed to relatively low field strength radiation simply due to the reduced coverage from sampling the SIM waveform.

The variable of interest for tests 1 to 8 was the replication of physical nodes. These tests were intended to examine possible differences in the susceptibility threshold of the nodes resulting from small differences in the way they were assembled and laid out in the chamber. The data from these tests was used to rank the physical nodes by their susceptibility thresholds.

Tests 1 and 10 to 16 examined the relative differences in the strength of the local field at each of the established node positions in the reverberation chamber. The intent was to assess the effectiveness of the stirrers in achieving a uniform field strength distribution throughout the chamber.

Tests 18 to 22 were added to the HSTC plan to examine the impact of the power cable routing from the end-cap to the node's in-stack power supply (see Figure 10). These tests were intended to determine the impact of the physical layout of a node on its susceptibility threshold. Figures 11 to 14 show the routings 1 to 4, respectively, used for these tests. Notice that tests 18 to 21 used the same node 8, while test 22 used node 7 as this test was intended as a check to see if the results for node 8 also applied to other nodes.

Two changes were added to the test procedure in order to protect the nodes from additional damage to the in-stack power supplies. First, the current drawn by the radiated node from the AC-to-DC power supply in the Control Room was constantly monitored by the Test Controller, and a test would be stopped automatically if the current exceeded a predetermined threshold set based on earlier observations of in-stack power supply failures. The second change was to monitor the state snapshots sent out by the radiated node (see report [2]) for any indication that its internal voltage level monitor triggered a reset. The voltage monitor on the CPU board was a built-in function that ensured that the board was allowed to run only when the input voltage was above a preset level. A reset triggered by the voltage monitor during a radiation round was viewed as an indication that the in-stack power supply was being overwhelmed by the radiation and that continued exposure would lead to a permanent failure. A policy was implemented on the monitoring system by which the second detected voltage-monitor triggered reset would stop the round. After an event of this kind, no additional testing would be performed at or above the current field strength level at the current frequency.

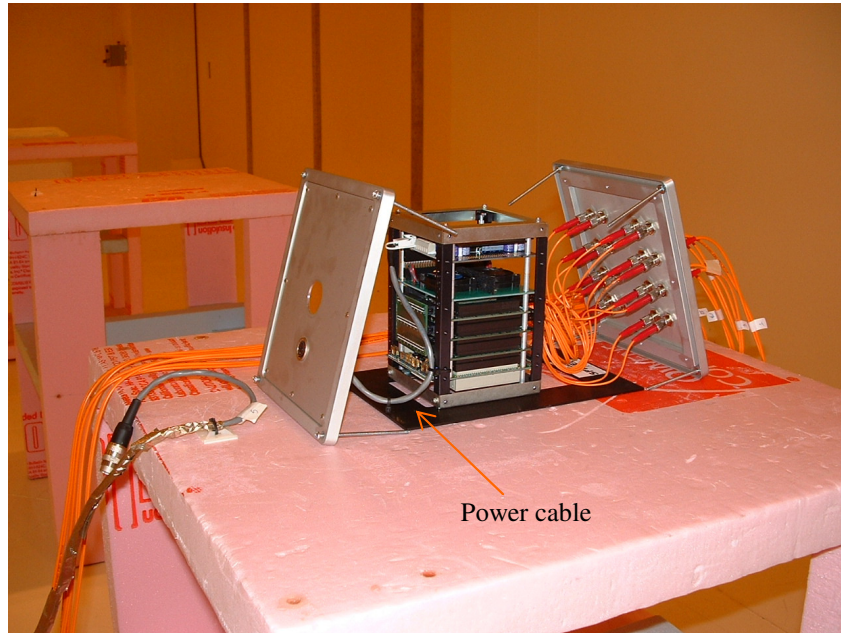


Figure 10: Physical layout of a node in the reverberation chamber

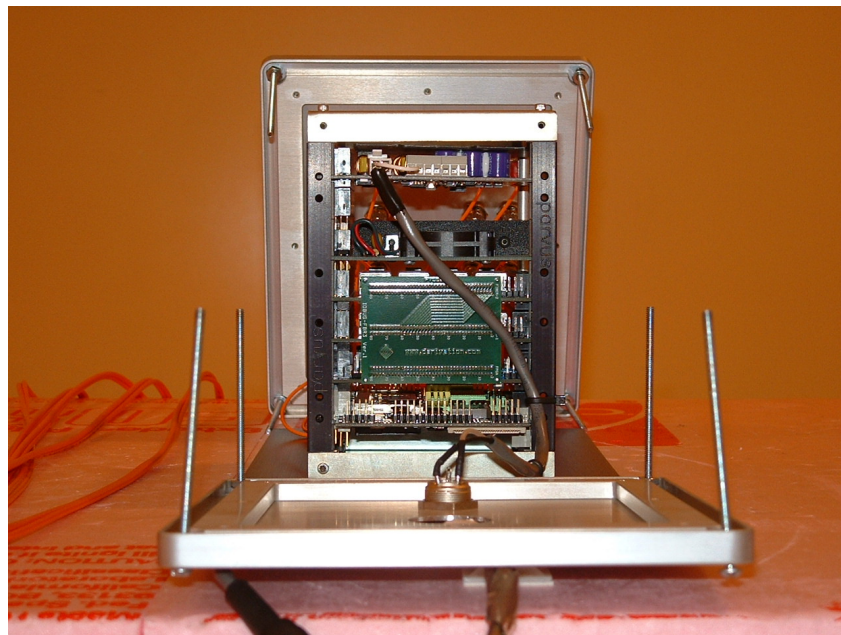


Figure 11: Power cable routing 1

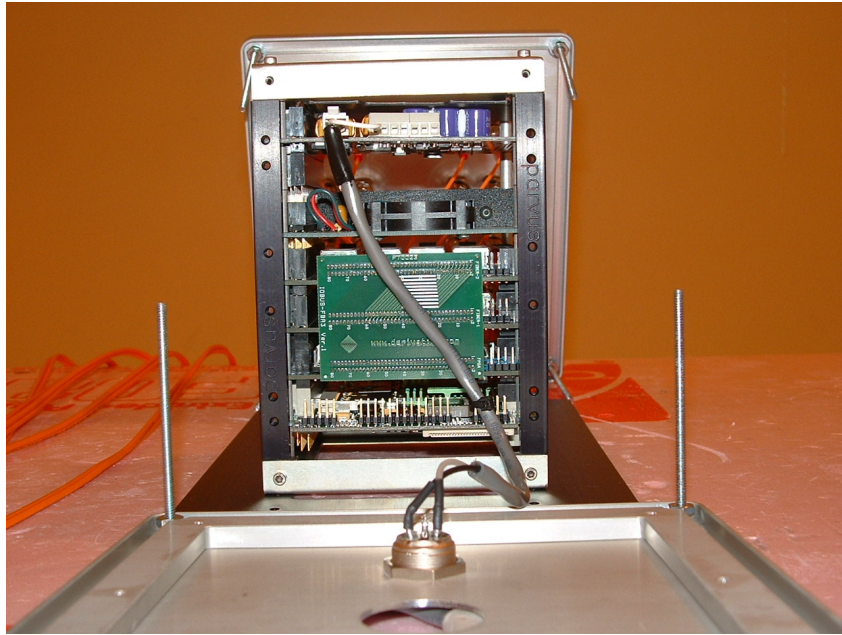


Figure 12: Power cable routing 2



Figure 13: Power cable routing 3



Figure 14: Power cable routing 4

4. Results and Analysis

This section is divided in four parts covering the results of the power cable routing tests, the modulation tests, the physical node tests and the chamber position tests.

4.1. Power Cable Routing

Figure 15 shows the measured susceptibility threshold profile for HSTC tests 18 to 22 in which the variable of interest was the routing of the power cable. The figure shows that the susceptibility threshold was lowest below 200 MHz and between 316.23 MHz and 510.9 MHz. The frequencies below 200 MHz had the lowest susceptibility thresholds, and there is a trend by which the susceptibility threshold increases with the frequency. Also notice that the two extreme routings (i.e., 1 and 4) resulted in the least susceptible (i.e., highest threshold) layouts, with routing 4 being the least susceptible. Routings 2 and 3 resulted in very similar susceptibility threshold profiles across the tested frequency range, and routing 3 was the most susceptible. In addition notice that the susceptibility profiles for nodes 7 and 8 with routing 2 differ by a small amount at most frequencies.

Comparing these susceptibility profiles with the routings shown in Figures 11 to 14, it seems that the susceptibility threshold is related to amount of overlap between the power cable and green side-board. This side-board carried low-voltage bit-serial data signals between the FPGA board and the fiber-optic transceiver modules (see reports [1] and [2]). Therefore, it was conjectured that the susceptibility threshold was determined by a coupling of radiated energy from the power cable to the signal wires on this side-board.

The other HSTC tests were conducted with power cable routings somewhere in between routings 2 and 3.

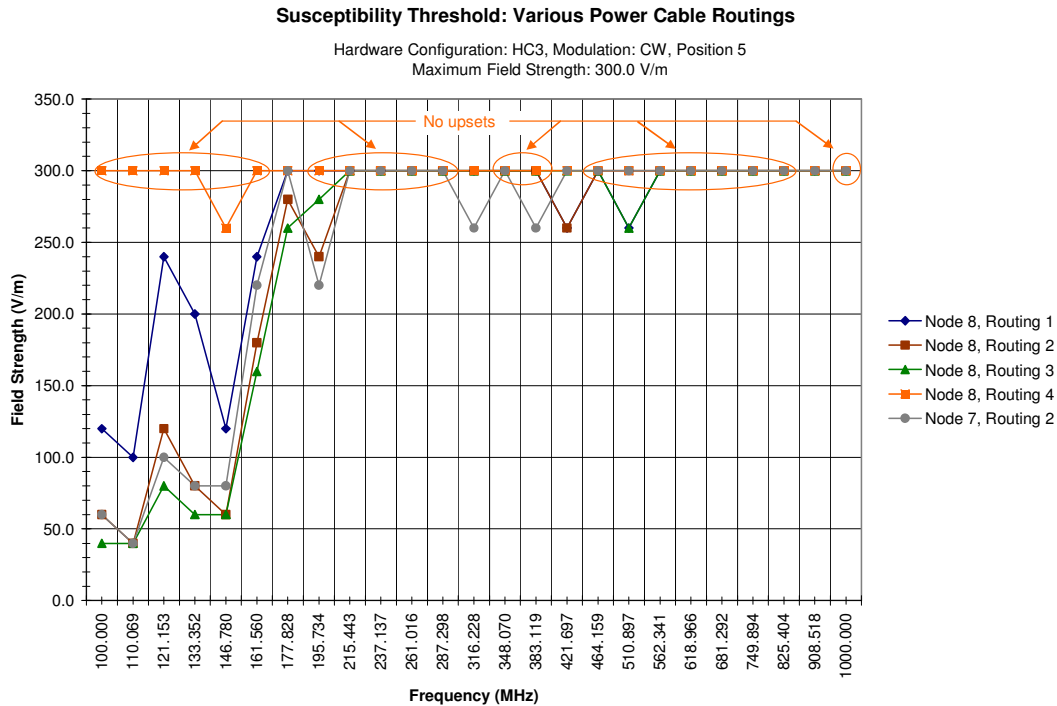


Figure 15: Measured susceptibility thresholds with variation in the node’s power cable routing

4.2. Modulation

Figure 16 shows the measured susceptibility threshold profiles for tests 1, 9 and 17 with variation in the amplitude modulation applied to the input signal driving the transmit antenna. The empty markers indicate that susceptibility was not detected at the maximum field strength level. The results show that the node was most susceptible below 200 MHz for every modulation. The second most susceptible frequency interval is from 383.12 MHz to 510.9 MHz.

Interestingly, the measured susceptibility profiles for all the modulations were very similar despite the fact that there are very large differences in duty cycles: 2% for pulse, 50% for square wave, and 100% for CW. A low duty cycle implies a low coverage of the SIM waveform (i.e., the node is exposed to only a small part of the SIM), which was thought to be a strong determining factor in the local field experienced by a radiated node and the measured susceptibility threshold. This result may seem to contradict observations made during the earlier versions of the HSTC in which pulse amplitude modulation like the strike pattern shown in Figure 4 reduced the repeatability of the susceptibility threshold measurements. However, there is one important difference between the earlier strike patterns and the modulations used here in that, in effect, only stroke-level modulation was used in tests 1, 9 and 17, and there was no strike-level modulation. Crucially, the stroke-level amplitude modulation was at a frequency of 1 KHz (i.e., 1 ms period) versus the multi-second periods for the strike-level modulations. Thus, with no strike-level

modulation, the stroke-level modulations were in effect sampling the SIM waveform at a high rate (i.e., 10,000 samples per stirrer revolution). We believe that this allowed the field strength amplitude experienced by the node in each test to follow closely the profile of the SIM waveform. It seems that it is not only the total coverage that matters, but also how that coverage is distributed in time. Also, it is known that for some electronic systems, the dwell time is an important determinant of susceptibility [22]. Evidently, the shortest dwell time of 20 μs on-time with pulse modulation was larger than the minimum dwell time needed to trigger HIRF-induced effects in our prototyping platform nodes. Report [23] offers additional insight into the effect of signal modulation on the measured susceptibility threshold of a device.

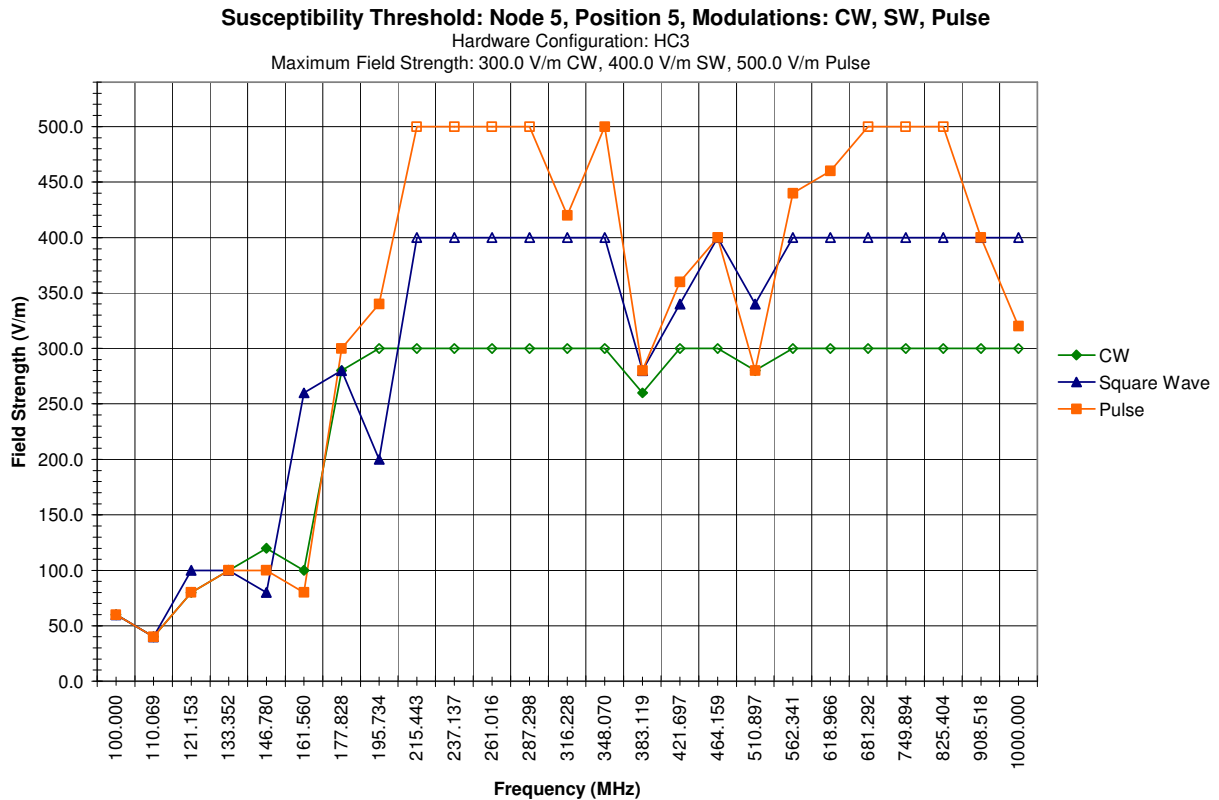


Figure 16: Measured susceptibility thresholds with variation in the chamber’s input modulation

If the reasoning described above is correct, some of the differences in the measured susceptibility thresholds probably had little to do with the modulation pattern and may be due to other still unexplained phenomena. For example, there is a range of variation of 180 V/m in the susceptibility thresholds measured at 161.56 MHz and 140 V/m at 195.73 MHz. The sudden drop in the threshold at 908.52 MHz and 1000 MHz for pulse modulation is also interesting. These variations are probably not related to the power cable routing because the tests used the same node with the same layout at the same position in the chamber. We suspect that these differences were due to the SIM waveforms being different in profile and peak amplitude in each of the tests. This experiment used a calibrated field-strength technique by which the recorded field strength during a radiation test was determined from a pre-test calibration of the input power required to generate a desired field-strength level at the receive antenna some distance away from where the nodes were positioned (see Figure 2 and Section 4.3 of report [1]). Thus, if the SIM waveforms during calibration and test were different, the actual field strength during a test could be different from the

calibrated strength. Likewise, if different tests had different SIM waveforms, the measured susceptibility threshold could be different.

The next step is to find a plausible explanation for variations in the SIM waveforms of different tests. For this, it helps to consider a radiated field inside a reverberation chamber and what happens when the field stirrers rotate. As described in report [1], a reverberation chamber is modeled as a large cavity resonator characterized by three-dimensional stationary wave patterns determined by the boundary conditions in the chamber (i.e., the relative position of the reflective surfaces inside chamber). The two mechanical field stirrers with reflective paddles (see Figures 2 and 3) change the boundary conditions and create different field structures as they rotate. The SIM waveform at a point in the chamber is the peak field-strength amplitude as the stirrers go around. Because of the complex field structure inside the chamber, the SIM waveform will be different at different points in the chamber. Furthermore, different angular offsets of the stirrers (see Figure 17) correspond to different boundary conditions, which create different field structures, which in turn produce different SIM waveforms. During the tests, the stirrers rotated at the same rate and maintained a constant angular offset relative to each other. Other than that, none of the HSTC tests controlled or specified this variable, and the tests did not measure the relation between the SIM waveforms and the relative angular offset of the stirrers. A future report will examine the relation between the SIM waveform characteristics and the angular offset of the stirrers using data collected after the HSTC test was completed.

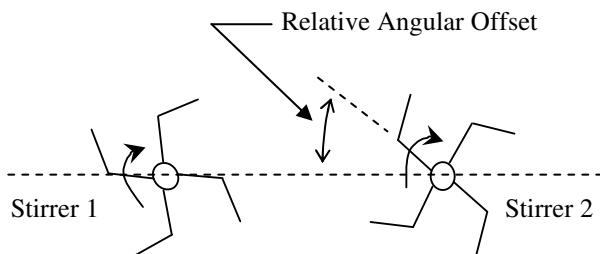


Figure 17: Illustration of relative angular offset for a pair of field stirrers rotating at the same speed

4.3. Physical Nodes

Figure 18 shows the susceptibility threshold results for HSTC tests 1 to 8 for physical nodes 1 to 8. The figure shows that there were three frequency intervals with susceptibility at or below the 300 V/m maximum nominal field strength with CW modulation. The interval from 100 MHz to 195.73 MHz had the lowest susceptibility thresholds and there is a common trend of minimum thresholds near 100 MHz and increasing with frequency. The variability of the susceptibility threshold in this interval seems to increase as the average susceptibility threshold increases. There is additional susceptibility in the interval from 316.23 MHz to 510.9 MHz, and at frequency 908.52 MHz, but there is no obvious pattern to the susceptibility at these frequencies. There was no measured susceptibility for 11 of 25 tested frequencies. Based on the results shown in Figure 16, we would expect the susceptibility thresholds for most of those 11 frequencies to be at around 500 V/m or less.

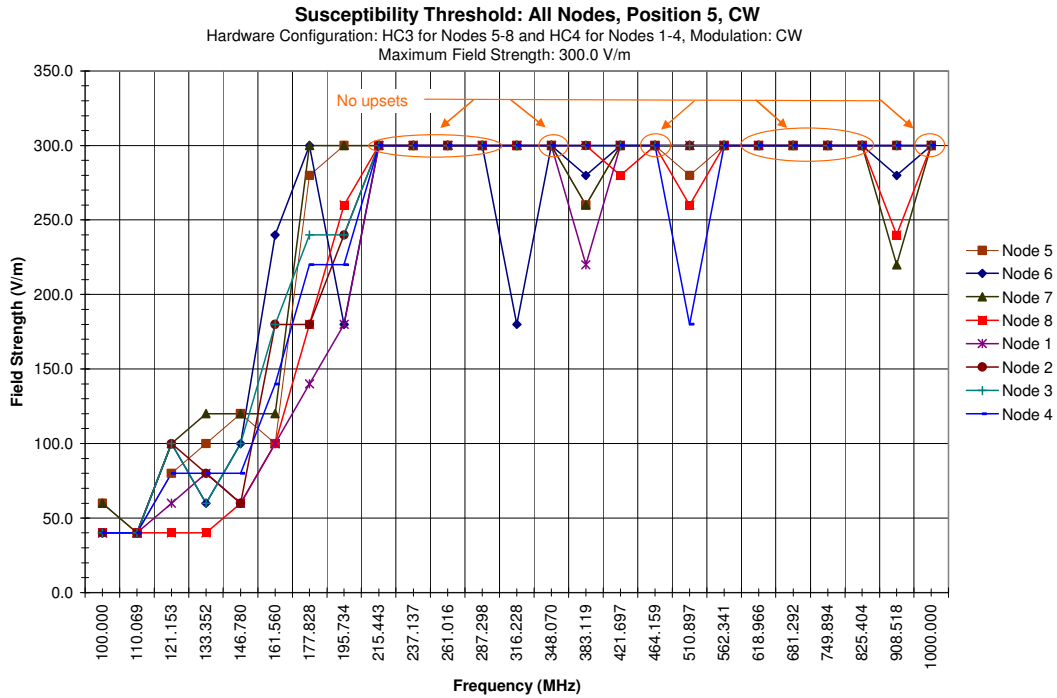


Figure 18: Measured susceptibility thresholds for all physical nodes using CW

Figures 19 and 20 separate the measured susceptibility thresholds for nodes 5 to 8 and 1 to 4, respectively. Each of the nodes 5 to 8 was programmed as RMU1 while being tested in configuration HC3, and nodes 1 to 4 were programmed as BIU1 in configuration HC4. All the nodes were tested at position 5 in the chamber. The RMUs showed susceptibility in three separate test frequency intervals and there was no susceptibility at 12 of the 25 test frequencies. The BIUs showed susceptibility below 200 MHz and at 383.12 and 510.9 MHz, and no susceptibility was observed at 15 test frequencies. The data does not offer any additional insight into differences between nodes programmed as RMUs or BIUs. Overall, the differences in measured susceptibility thresholds are probably due to slight differences in the routing of the power cables or the SIM waveforms generated by the chamber. Another possible cause for the differences in measurements could be the power output from the amplifier driving the transmit antenna. A diagram of the chamber test setup is shown in Figure 7 of report [1]. The power amplifier is designed to maintain a constant input-output gain, but this is complicated by the time-varying electromagnetic characteristics of the chamber as the stirrers rotate [23]. No data was collected during this experiment to examine this possible source of error in measured susceptibility thresholds.

Table 4 shows the analysis for ranking the physical nodes by their measured susceptibility threshold. At each frequency, the nodes were ranked by increasing susceptibility threshold by assigning order indices from 1 to 8. Nodes with the same susceptibility threshold were assigned the same ranking index. A no-upset result at a specific frequency was assigned a ranking of 8. The frequencies at which none of the nodes showed susceptibility were removed from consideration. Nodes 5 and 7 had the same mean ranking. The overall ranking of nodes was as follows, by node id: 1, 8, 4, 6, 2, (5, 7), 3. Nodes 1 to 4 as BIUs ranked as follows: 1, 4, 2, 3. For nodes 5 to 8 as RMUs, the ranking was: 8, 6, (5, 7).

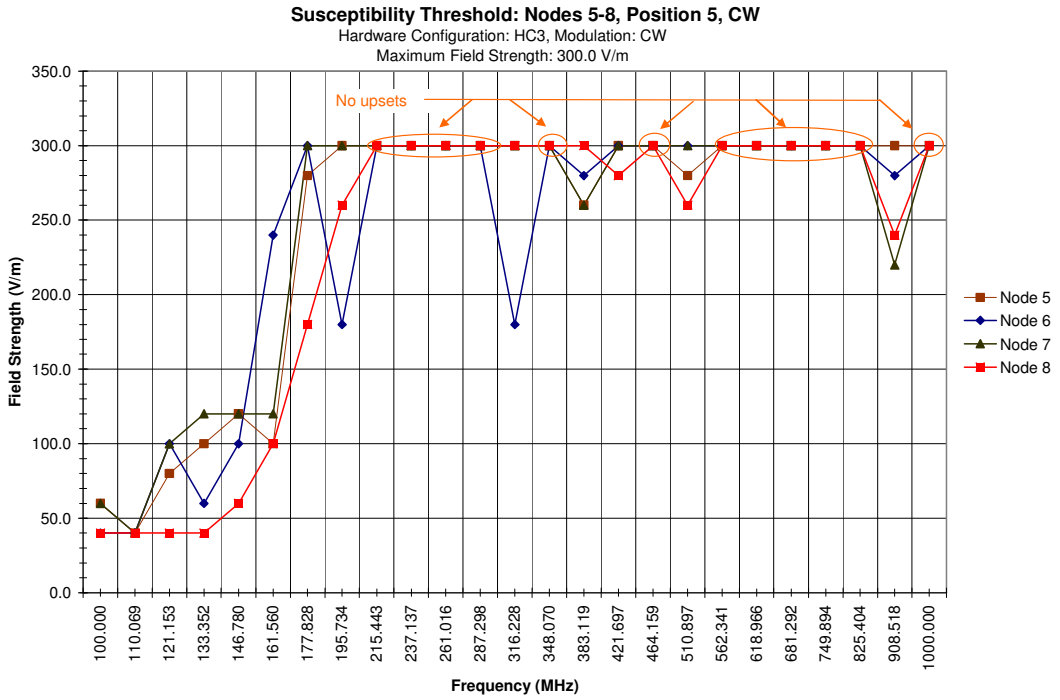


Figure 19: Measured susceptibility threshold for physical nodes 5 to 8 programmed as RMUs

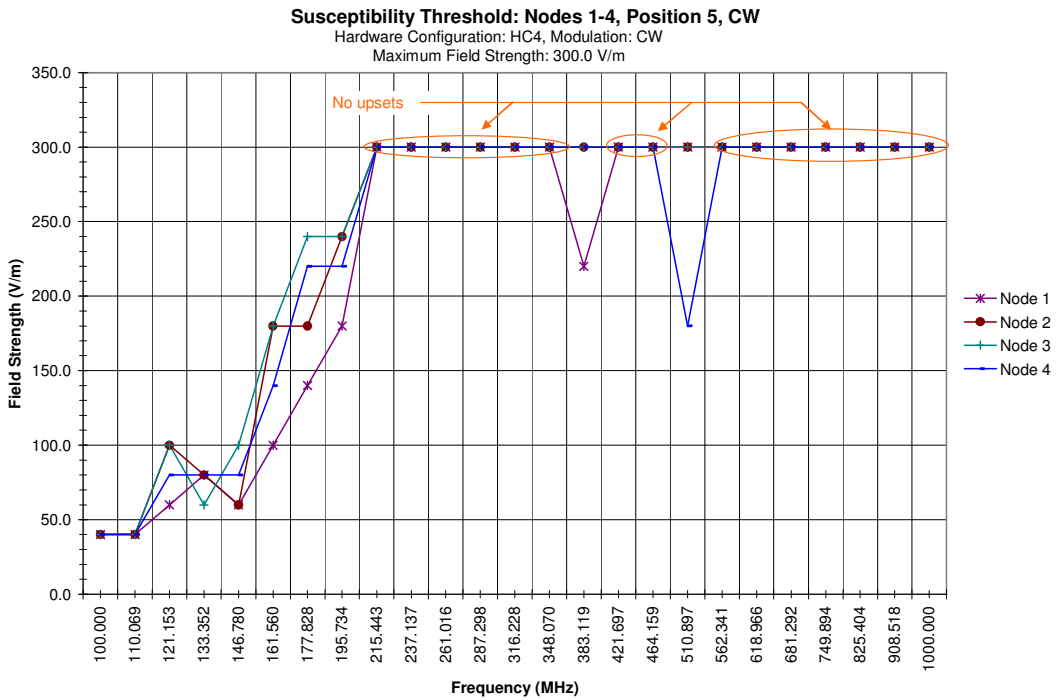


Figure 20: Measured susceptibility threshold for physical nodes 1 to 4 programmed as BIUs

Table 4: Worksheet for ranking physical RSPP nodes by measured susceptibility threshold

All nodes at position 5, Modulation: CW																	
Frequency	Susceptibility Threshold Field Strength (V/m)								Susceptibility Threshold Rank (Lowest = 1 to Highest = 8)								
	Node 1	Node 2	Node 3	Node 4	Node 5	Node 6	Node 7	Node 8	Node 1	Node 2	Node 3	Node 4	Node 5	Node 6	Node 7	Node 8	
100.000	40.0	40.0	40.0	40.0	60.0	40.0	60.0	40.0	1	1	1	1	7	1	7	1	
110.069	40.0	40.0	40.0	40.0	40.0	40.0	40.0	40.0	1	1	1	1	1	1	1	1	
121.153	60.0	100.0	100.0	80.0	80.0	100.0	100.0	40.0	2	5	5	3	3	5	5	1	
133.352	80.0	80.0	60.0	80.0	100.0	60.0	120.0	40.0	4	4	2	4	7	2	8	1	
146.780	60.0	60.0	100.0	80.0	120.0	100.0	120.0	60.0	1	1	5	4	7	5	7	1	
161.560	100.0	180.0	180.0	140.0	100.0	240.0	120.0	100.0	1	6	7	5	1	8	4	1	
177.828	140.0	180.0	240.0	220.0	280.0	No upset	No upset	180.0	1	2	5	4	6	8	8	2	
195.734	180.0	240.0	240.0	220.0	No upset	180.0	No upset	260.0	1	4	4	3	8	1	8	6	
215.443	No upset	No upset	No upset	No upset	No upset	No upset	No upset	No upset									
237.137	No upset	No upset	No upset	No upset	No upset	No upset	No upset	No upset									
261.016	No upset	No upset	No upset	No upset	No upset	No upset	No upset	No upset									
287.298	No upset	No upset	No upset	No upset	No upset	No upset	No upset	No upset									
316.228	No upset	No upset	No upset	No upset	No upset	180.0	300.0	No upset	8	8	8	8	8	1	2	8	
348.070	No upset	No upset	No upset	No upset	No upset	No upset	No upset	No upset									
383.119	220.0	No upset	No upset	No upset	260.0	280.0	260.0	No upset	1	8	8	8	2	4	2	8	
421.697	No upset	No upset	No upset	No upset	No upset	No upset	No upset	280.0	8	8	8	8	8	8	8	1	
464.159	No upset	No upset	No upset	No upset	No upset	No upset	No upset	No upset									
510.897	300.0	No upset	No upset	180.0	280.0	No upset	No upset	260.0	4	8	8	1	3	8	8	2	
562.341	300.0	No upset	No upset	300.0	No upset	No upset	No upset	No upset	1	8	8	1	8	8	8	8	
618.966	No upset	No upset	No upset	No upset	No upset	No upset	No upset	No upset									
681.292	No upset	No upset	No upset	No upset	No upset	No upset	No upset	No upset									
749.894	No upset	No upset	No upset	No upset	No upset	No upset	No upset	No upset									
825.404	No upset	No upset	No upset	No upset	No upset	No upset	No upset	No upset									
908.518	No upset	No upset	No upset	No upset	No upset	280.0	220.0	240.0	8	8	8	8	8	3	1	2	
1000.000	No upset	No upset	No upset	No upset	No upset	No upset	No upset	No upset									
							Count of	1	8	3	2	4	2	4	2	7	
							Count of	2	1	1	1	0	1	1	2	3	
							Count of	3	0	0	0	2	2	1	0	0	
							Count of	4	2	2	1	3	0	1	1	0	
							Count of	5	0	1	3	1	0	2	1	0	
							Count of	6	0	1	0	0	1	0	0	1	
							Count of	7	0	0	1	0	3	0	2	0	
							Count of	8	3	6	6	4	5	5	6	3	
							Total Number of Rankings	14	14	14	14	14	14	14	14	14	
							Sum (Rank*Count)	42	72	78	59	77	63	77	43		
							Mean Rank	3.00	5.14	5.57	4.21	5.50	4.50	5.50	3.07		
							Overall Relative Susceptibility	1	5	8	3	6	4	6	2		
							BIU Relative Susceptibility	1	3	4	2	**	**	**	**		
							RMU Relative Susceptibility	**	**	**	**	3	2	3	1		

4.4. Chamber Positions

Figure 21 shows the measured susceptibility thresholds for nodes 1 to 8 at their default positions in the chamber by which the position id is the same as the node id. As in Figure 18 for position 5, susceptibility was detected in three frequency intervals: below 200 MHz, from 316.23 MHz to 510.9 MHz, and at frequency 908.52 MHz. The basic trends for the full set of positions remain the same compared to the trends at position 5 only. The most remarkable feature in Figure 21 compared to Figure 18 is the large variability in measured susceptibility thresholds between 146.78 MHz and 195.73 MHz. There is also a significant drop in the average susceptibility threshold at 195.73 MHz. Obviously, this simply means that average field strength at positions other than 5 was lower than at position 5 for frequencies around 146.78 MHz, and that the opposite was true near 195.73 MHz. (Recall that the reported field strength for a test round was the calibrated value, which represented an expected average throughout the chamber. The field was not measured and reported for each position individually.) However, we do not have insight about why this was so. We speculate that this may be due to inherent differences in the SIM patterns at the various positions and the limitations of the stirrers in achieving field uniformity throughout the chamber.

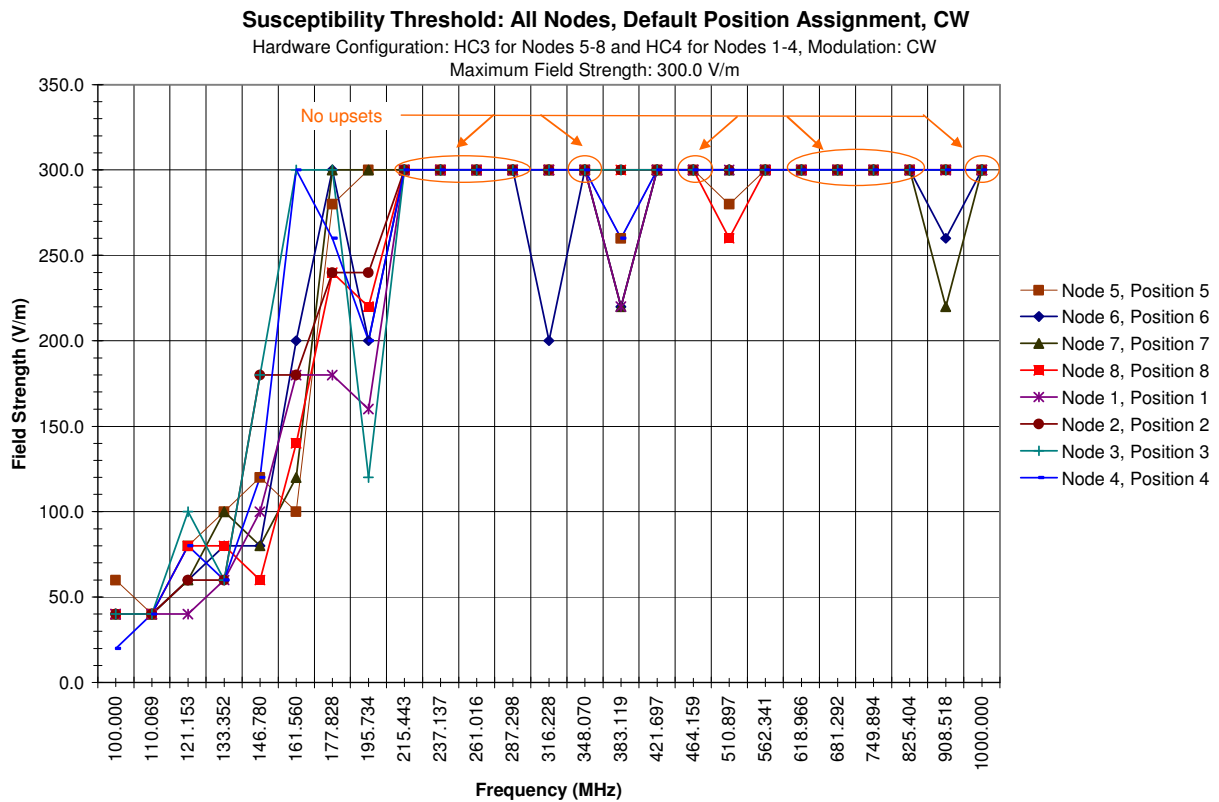


Figure 21: Measured susceptibility threshold for physical nodes 1 to 8 at their corresponding default positions

Table 5: Worksheet for ranking chamber positions by measured node susceptibility thresholds

Frequency	Field Scaling Ratio (wrt Position 5)								Field Strength Ranking (Lowest = 1 to Highest = 8)							
	Position 1	Position 2	Position 3	Position 4	Position 5	Position 6	Position 7	Position 8	Position 1	Position 2	Position 3	Position 4	Position 5	Position 6	Position 7	Position 8
100.000	1.000	1.000	1.000	2.000	1.000	1.000	1.500	1.000	1	1	1	8	1	1	7	1
110.069	1.000	1.000	1.000	1.000	1.000	1.000	1.000	1.000	1	1	1	1	1	1	1	1
121.153	1.500	1.667	1.000	1.000	1.000	1.667	1.667	0.500	5	6	2	2	2	6	6	1
133.352	1.333	1.333	1.000	1.333	1.000	0.750	1.200	0.500	6	6	3	6	3	2	5	1
146.780	0.600	0.333	0.556	0.667	1.000	1.250	1.500	1.000	3	1	2	4	5	7	8	5
161.560	0.556	1.000	< 0.6	0.467	1.000	1.200	1.000	0.714	2	5	3	1	5	8	5	4
177.828	0.778	0.750	< 0.8	0.846	1.000	≈ 1.0	≈ 1.0	0.750	3	1	4	5	6	7	7	1
195.734	1.125	1.000	2.000	1.100	≈ 1.0	0.900	> 1.0	1.182	6	2	8	5	3	1	4	7
215.443																
237.137																
261.016																
287.298																
316.228	≈ 1.0	≈ 1.0	≈ 1.0	≈ 1.0	≈ 1.0	0.900	< 1.0	≈ 1.0	3	3	3	3	3	1	2	3
348.070																
383.119	1.000	> 1.0	≈ 1.0	> 1.15	1.000	1.273	1.182	≈ 1.0	1	5	3	6	1	8	7	3
421.697	≈ 1.0	≈ 1.0	≈ 1.0	> 1.0	≈ 1.0	≈ 1.0	≈ 1.0	< 0.93	2	2	2	8	2	2	2	1
464.159																
510.897	< 1.0	≈ 1.0	> 1.0	0.600	1.000	≈ 1.0	> 1.0	1.000	2	5	7	1	3	5	7	3
562.341	< 1.0	≈ 1.0	≈ 1.0	< 1.0	≈ 1.0	≈ 1.0	≈ 1.0	≈ 1.0	1	3	3	1	3	3	3	3
618.966																
681.292																
749.894																
825.404																
908.518	≈ 1.0	≈ 1.0	> 1.0	≈ 1.0	≈ 1.0	1.077	1.000	0.800	4	4	8	4	4	3	2	1
1000.000																
							Count of	1	4	4	2	4	3	4	1	7
							Count of	2	3	2	3	1	2	2	3	0
							Count of	3	3	2	5	1	5	2	1	4
							Count of	4	1	1	1	2	1	0	1	1
							Count of	5	1	3	0	2	2	1	2	1
							Count of	6	2	2	0	2	1	1	1	0
							Count of	7	0	0	1	0	0	2	4	1
							Count of	8	0	0	2	2	0	2	1	0
							Total Number of Rankings	14	14	14	14	14	14	14	14	14
							Sum (Rank*Count)	40	45	50	55	42	55	66	35	
							Mean Rank	2.86	3.21	3.57	3.93	3.00	3.93	4.71	2.50	
							Overall Field Strength Ranking	2	4	5	6	3	6	8	1	
							Ranking for Positions 1-4	1	2	3	4 **	**	**	**	**	
							Ranking for Positions 5-8	**	**	**	**	2	3	4	1	

Table 5 shows the analysis performed to rank the chamber positions by the relative average of their local field strength as inferred from the measured susceptibility thresholds. The empty rows are for frequencies for which no node at any position or field strength experienced an upset. These frequencies were removed from consideration in the ranking analysis of the positions. Section 5.5 in report [1] describes the model and reasoning supporting this analysis. It is assumed that the susceptibility threshold with respect to the actual local field strength experienced by a node is an inherent property of the node in the sense that whether the node is susceptible or not is determined by the strength of the field relative to the threshold of the node. Therefore, ignoring errors due to the measurement being carried out in a mode-stirred reverberation chamber, the difference in susceptibility thresholds measured at two different positions in the chamber is directly related to the relative strength of the field at these positions. A lower field strength will result in a higher measured susceptibility threshold, and vice versa. The ratio of the susceptibility thresholds is inversely proportional to the ratio of the field strengths. The field scaling ratio on the top left part of Table 5 measures the strength of the field at position x relative to position 5, which is the reference position. To handle cases in which no susceptibility was detected at a particular test frequency, it is assumed that the threshold was 300 V/m to compute the ratio, which is then complemented with a smaller than ($<$), larger than ($>$), or approximately equal (\approx) sign depending on whether the denominator, numerator, or both are assumed to be 300 V/m. These signs are used in ranking the field ratios at each particular frequency, as shown on the top right side of Table 5. The average ranking results are shown on the bottom right part of Table 5. The overall ranking was as follows, with positions 4 and 6 tied in sixth place: 8, 1, 5, 2, 3, (4, 6), 7. For position 1 to 4 which are used for nodes 1 to 4, the computed average ranking was: 1, 2, 3, 4. For positions 5 to 8 used for nodes 5 to 8, the ranking was: 8, 5, 6, 7.

An interesting observation is that the mean of the field strength ratios in Table 5 is 1.014, with a maximum of 2.000 and a minimum of 0.333. This gives a better sense of the performance of the mode-stirred reverberation chamber relative to the uniformity of the peak field strength and the error range in measurements of susceptibility thresholds.

It is known that the large measurement errors in the mode-stirred reverberation chamber make unreliable the computed rankings of nodes and positions and that using them to match the susceptibility thresholds of the configurations in the HEC part of the experiment may not produce the desired effect of reducing possible biases in the HEC data due to differences in susceptibility thresholds. Still, this approach was used because it is a simple methodical way of assigning ROBUS-2 functions to physical nodes and physical nodes to chamber positions. The configurations and results of the HEC experiment will be presented in a future report.

5. Final Remarks

An important motivation for the HSTC experiment was to have an opportunity to familiarize ourselves with the intricacies of using a reverberation chamber to generate functional system upsets suitable for the study of fault response in safety-critical systems. In the HSTC experiment, we examined how the layout of a physical node determines its susceptibility to HIRF and how the susceptibility profile of a node changes with the radiation frequency and modulation. We also examined differences in the susceptibility threshold profiles of a set of physical nodes due to slight differences in the way the nodes are assembled and laid out in the chamber. Additionally, we investigated differences in the local HIRF environment at various locations in the chamber. The HSTC experience enabled us to uncover the field amplitude modulation mechanism by which the mode stirrers homogenize the HIRF environment. This experience

has given us a better understanding of the operation of the reverberation chamber and allowed us to develop a safe and reliable test methodology that has already proven its value in a collaborative research effort [19, 20, 21].

The results of the HSTC were used in the planning of the HEC experiment. The results of the HEC will be presented in a series of future reports. We will also report on analysis carried out to characterize the SIM phenomenon with respect to various parameters, including the angular offset of the mode stirrers.

The Appendix presents the susceptibility threshold data collected during the HSTC experiment.

Appendix A. Test Data

Figures A.1 to A.22 show the susceptibility threshold measurements for the HSTC tests. Empty markers in the figures indicate that the susceptibility threshold was larger than the maximum field strength of 300 V/m.

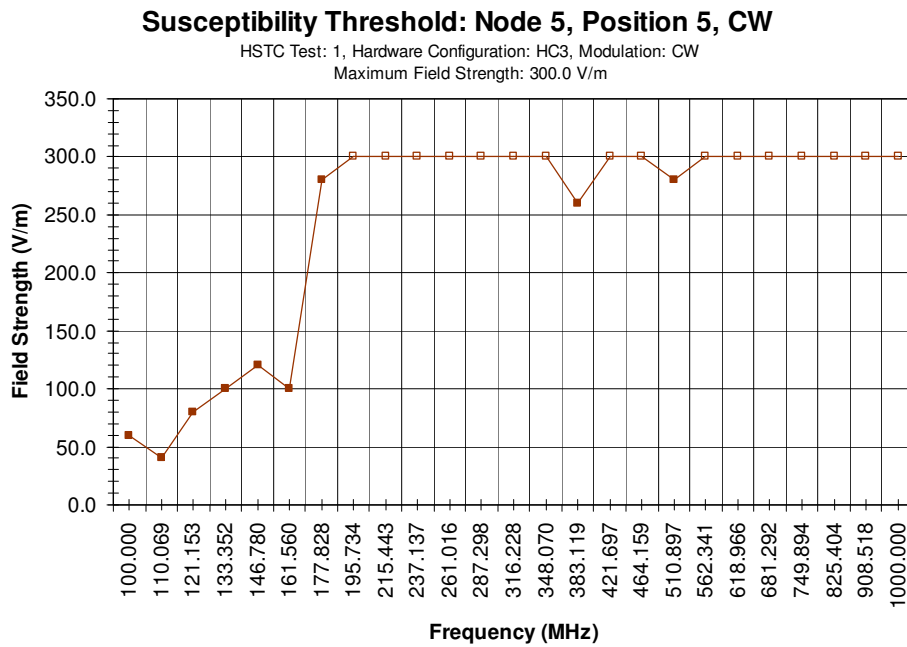


Figure A.1: Measured susceptibility profile for HSTC Test 1

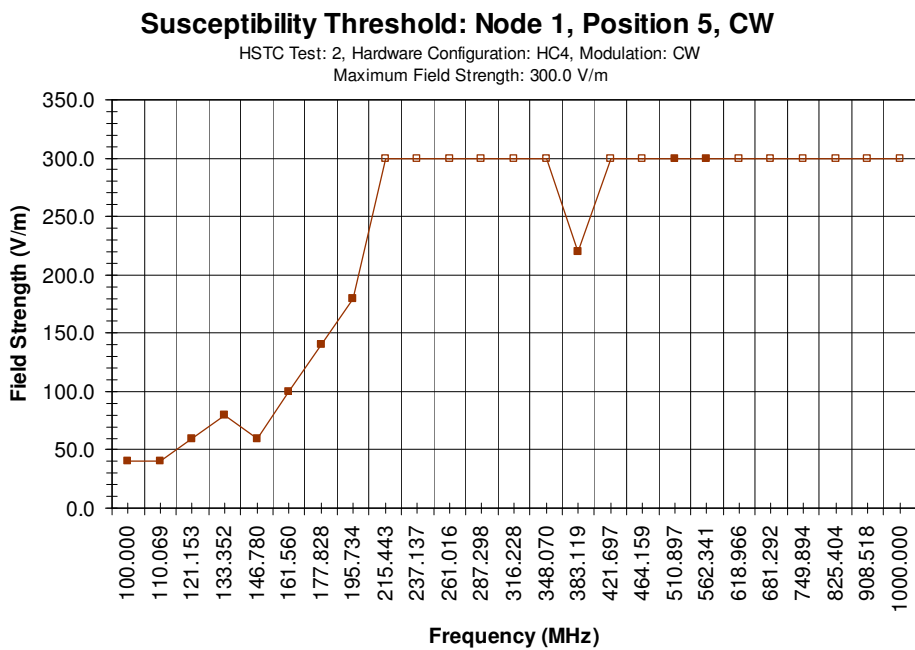


Figure A.2: Measured susceptibility profile for HSTC Test 2

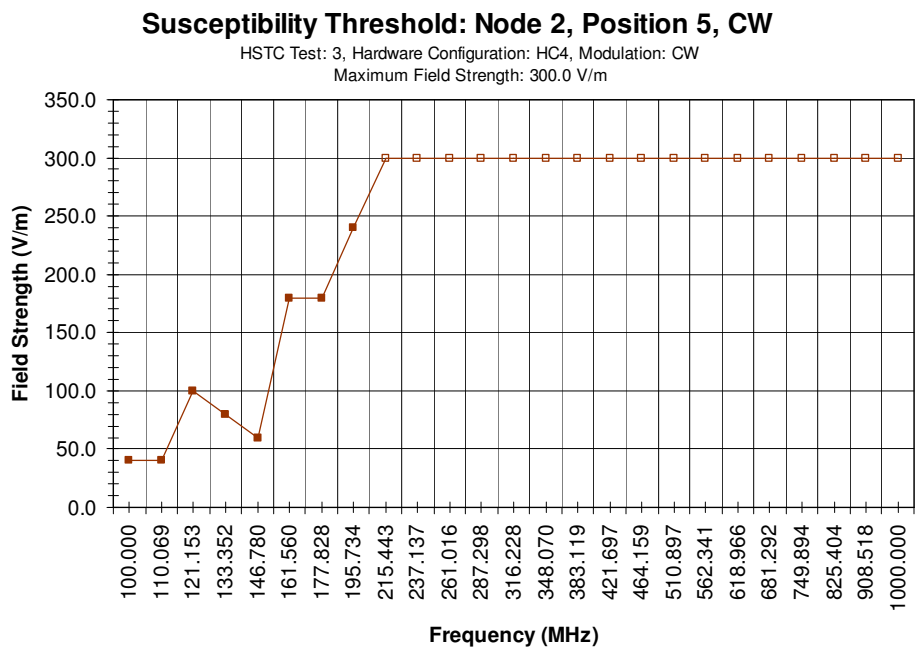


Figure A.3: Measured susceptibility profile for HSTC Test 3

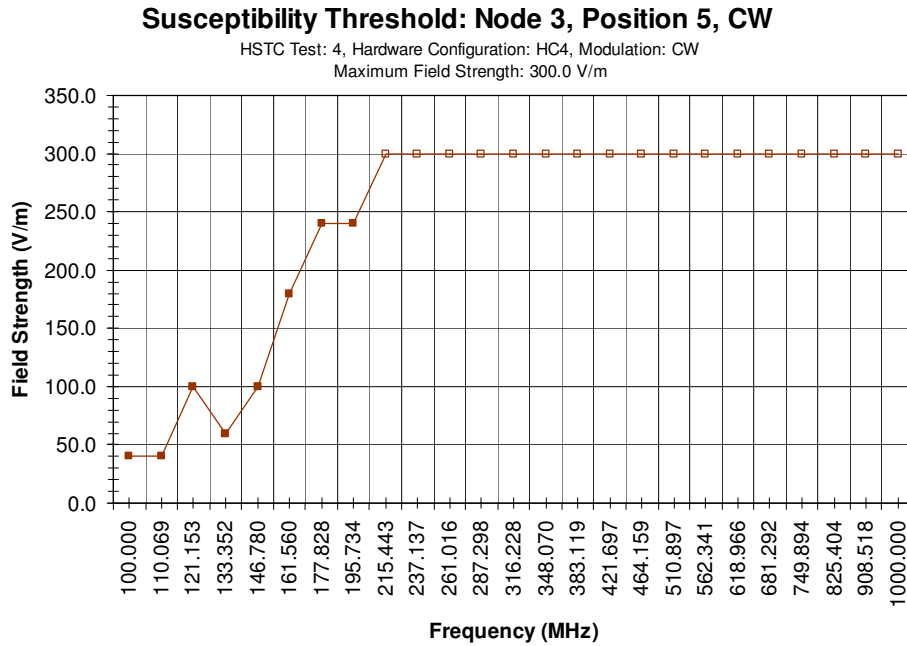


Figure A.4: Measured susceptibility profile for HSTC Test 4

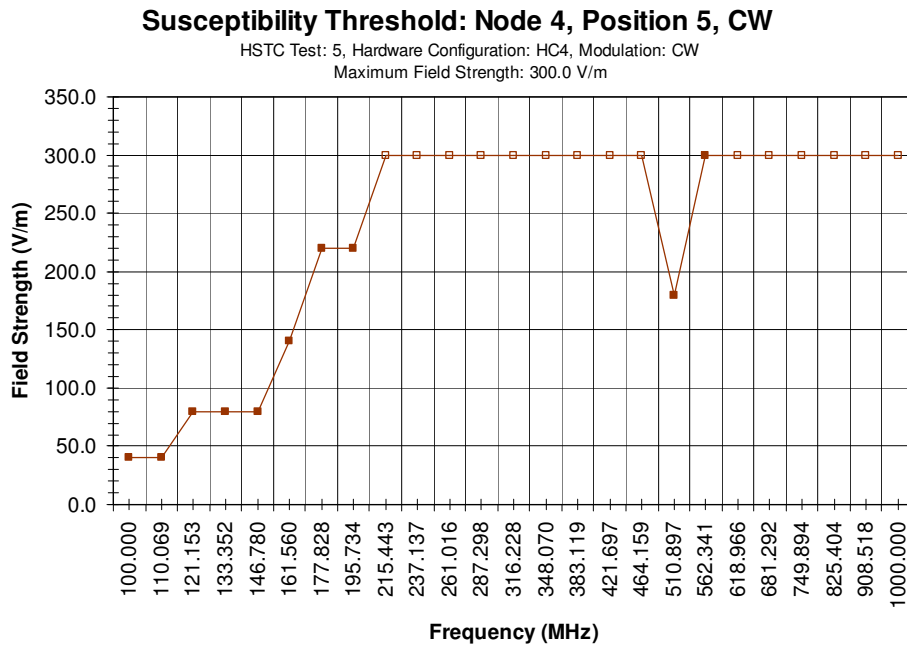


Figure A.5: Measured susceptibility profile for HSTC Test 5

Susceptibility Threshold: Node 6, Position 5, CW

HSTC Test: 6, Hardware Configuration: HC3, Modulation: CW
Maximum Field Strength: 300.0 V/m

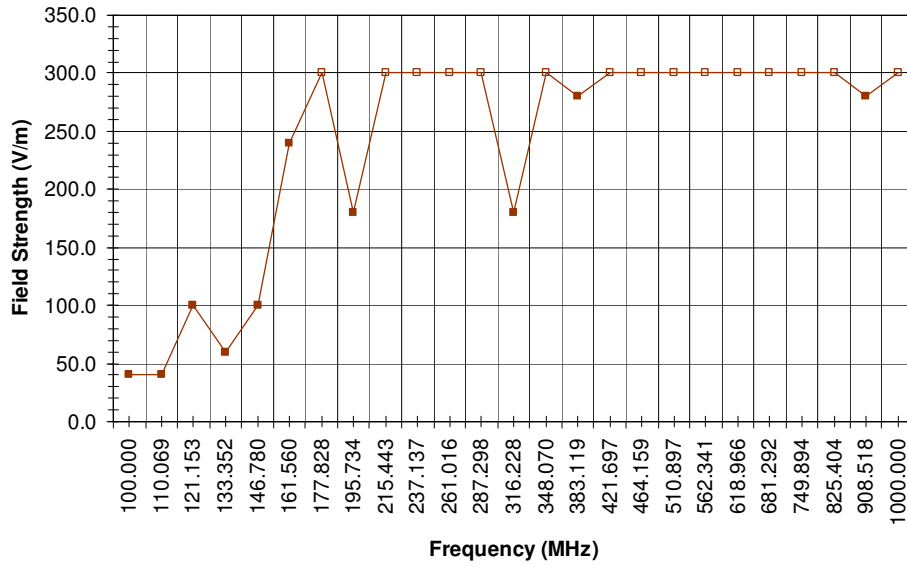


Figure A.6: Measured susceptibility profile for HSTC Test 6

Susceptibility Threshold: Node 7, Position 5, CW

HSTC Test: 7, Hardware Configuration: HC3, Modulation: CW
Maximum Field Strength: 300.0 V/m

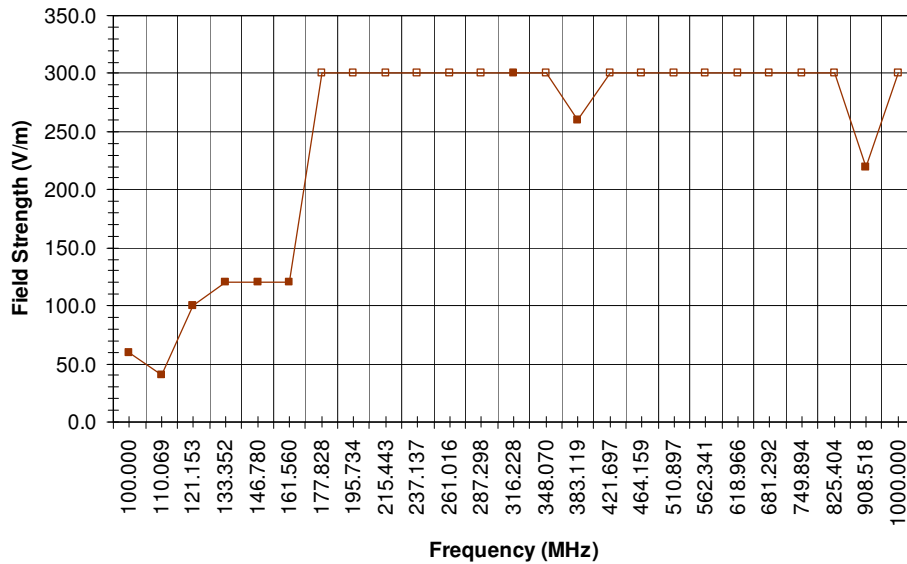


Figure A.7: Measured susceptibility profile for HSTC Test 7

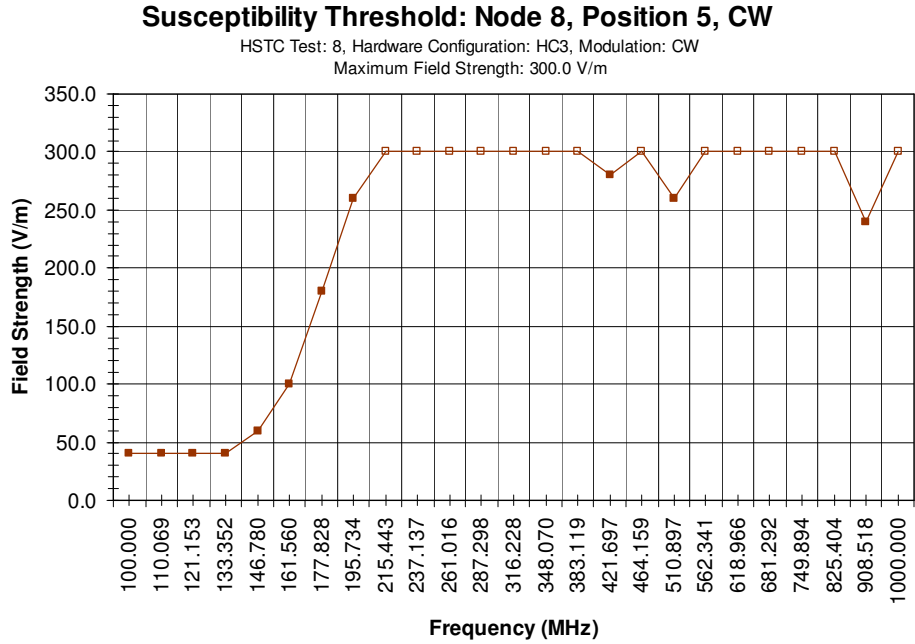


Figure A.8: Measured susceptibility profile for HSTC Test 8

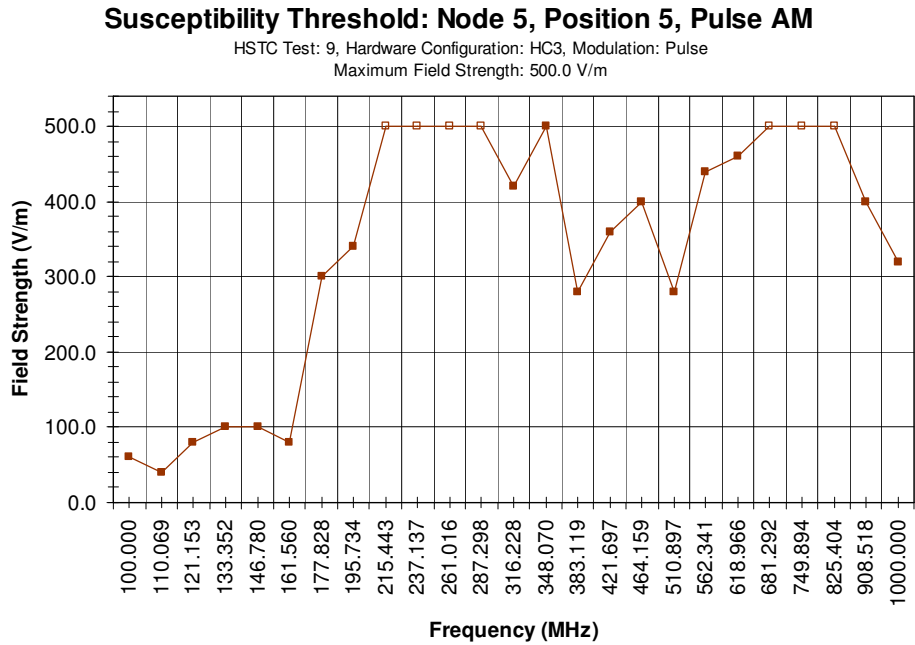


Figure A.9: Measured susceptibility profile for HSTC Test 9

Susceptibility Threshold: Node 1, Position 1, CW

HSTC Test: 10, Hardware Configuration: HC4, Modulation: CW
Maximum Field Strength: 300.0 V/m

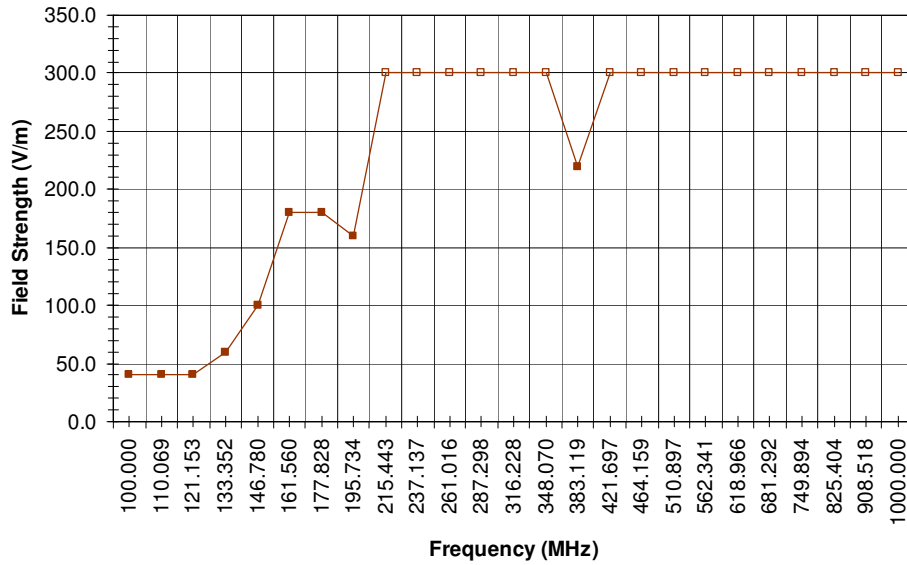


Figure A.10: Measured susceptibility profile for HSTC Test 10

Susceptibility Threshold: Node 2, Position 2, CW

HSTC Test: 11, Hardware Configuration: HC4, Modulation: CW
Maximum Field Strength: 300.0 V/m

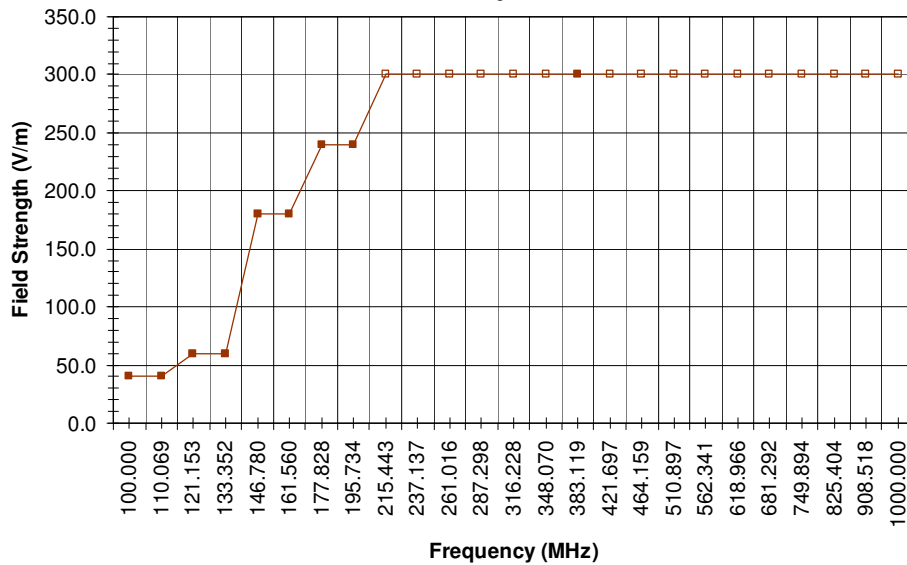


Figure A.11 Measured susceptibility profile for HSTC Test 11

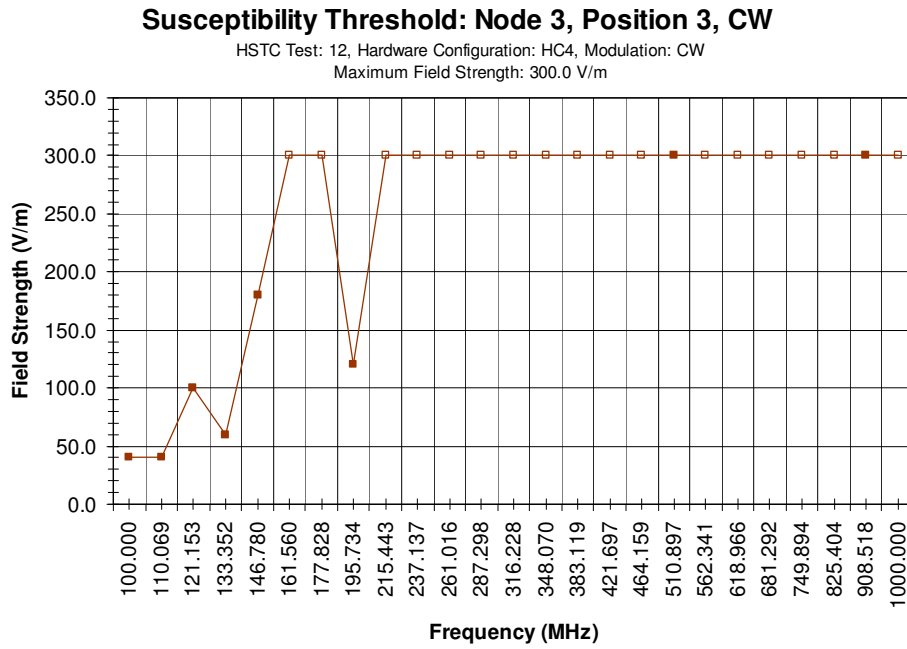


Figure A.12: Measured susceptibility profile for HSTC Test 12

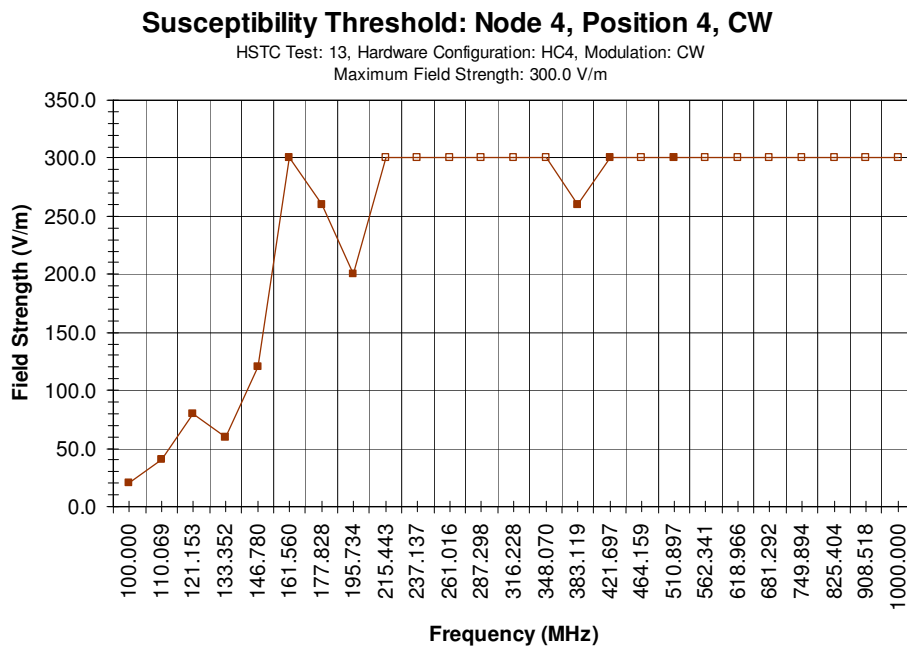


Figure A.13: Measured susceptibility profile for HSTC Test 13

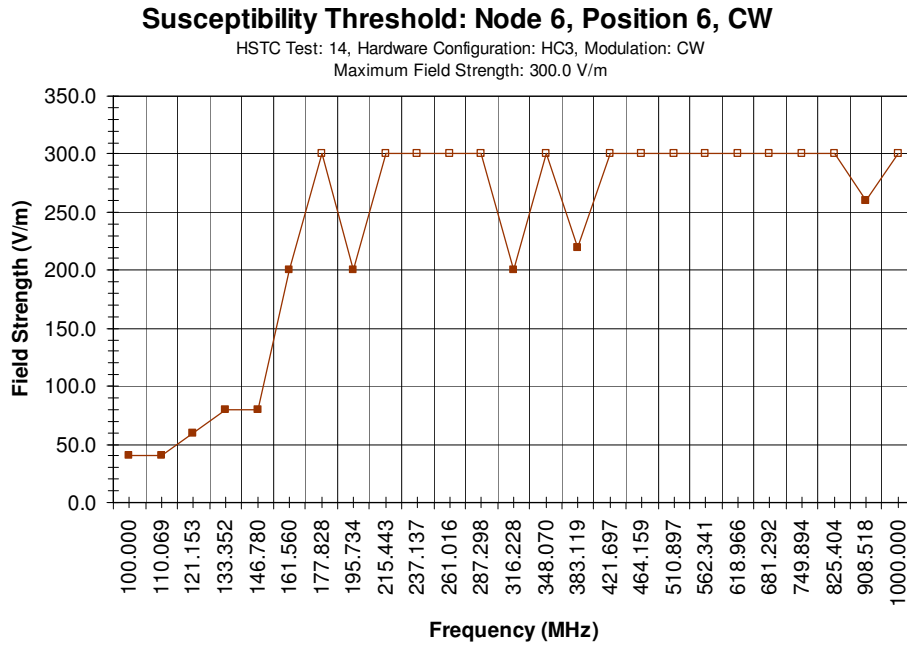


Figure A.14: Measured susceptibility profile for HSTC Test 14

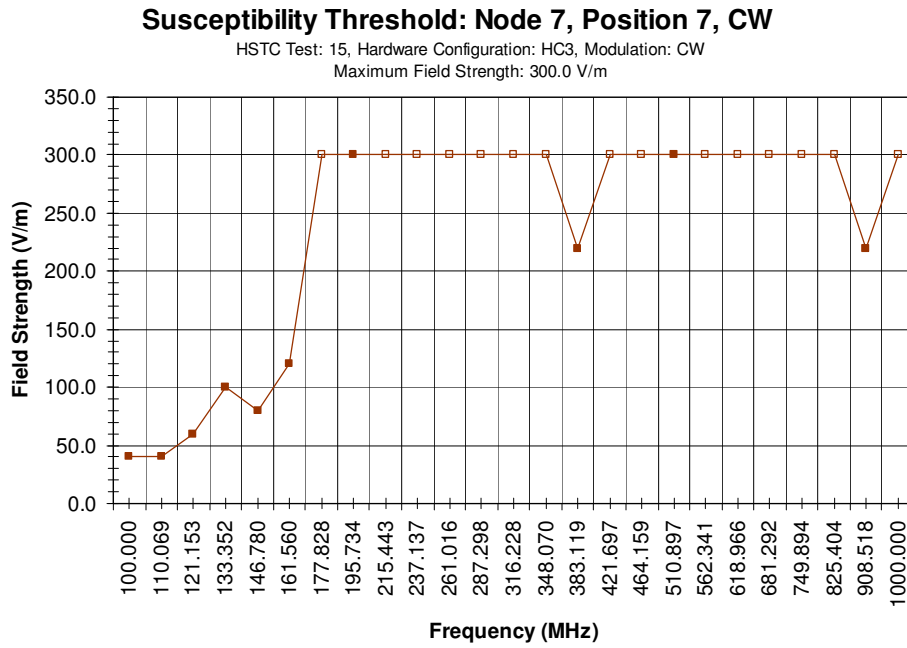


Figure A.15: Measured susceptibility profile for HSTC Test 15

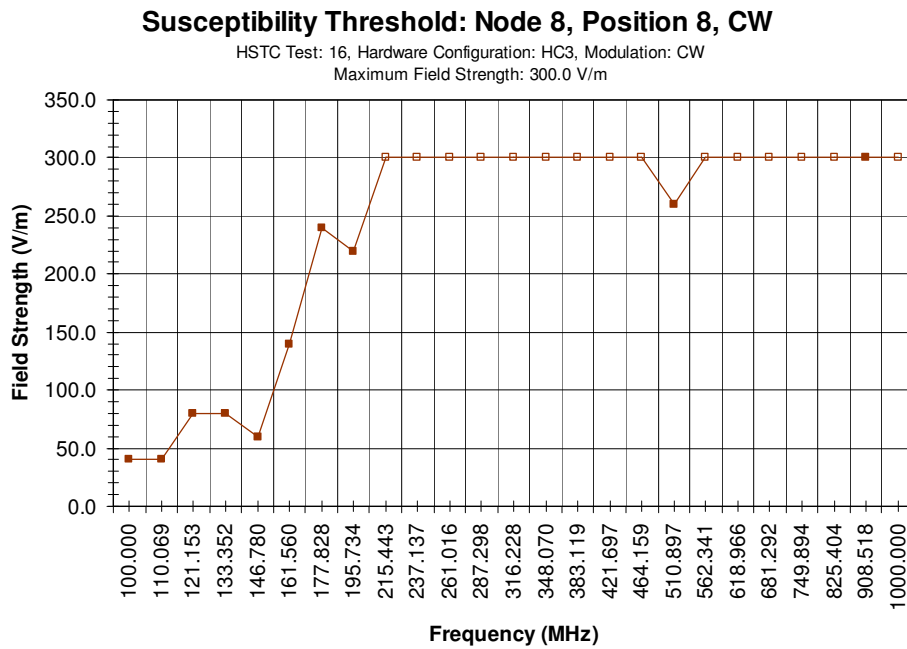


Figure A.16: Measured susceptibility profile for HSTC Test 16

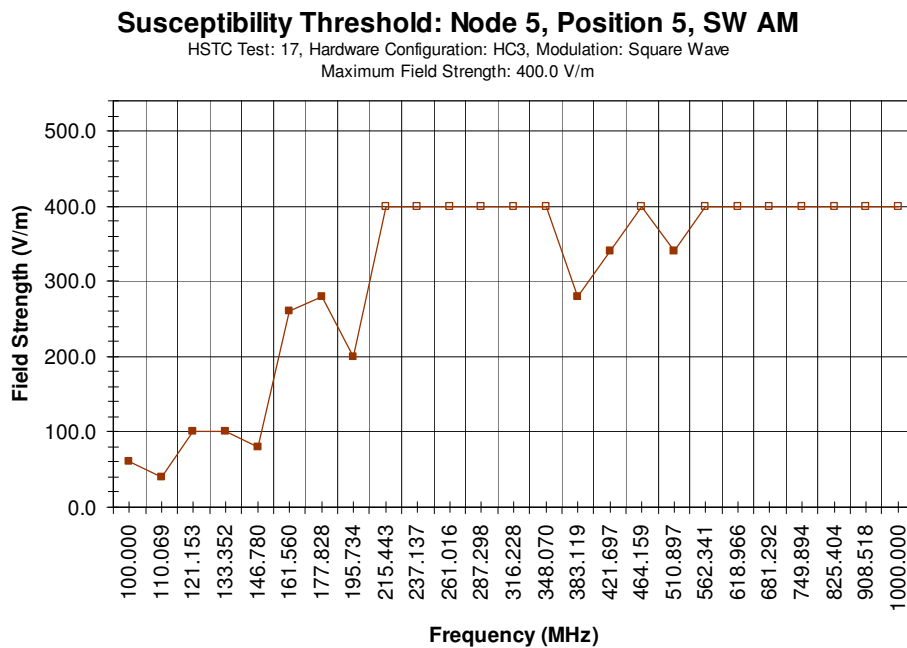


Figure A.17: Measured susceptibility profile for HSTC Test 17

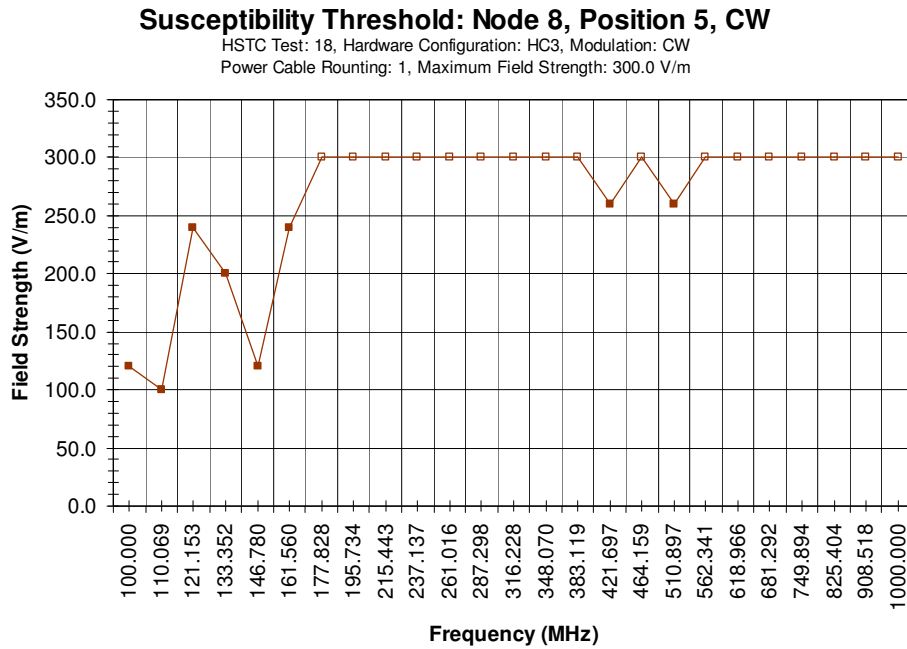


Figure A.18: Measured susceptibility profile for HSTC Test 18

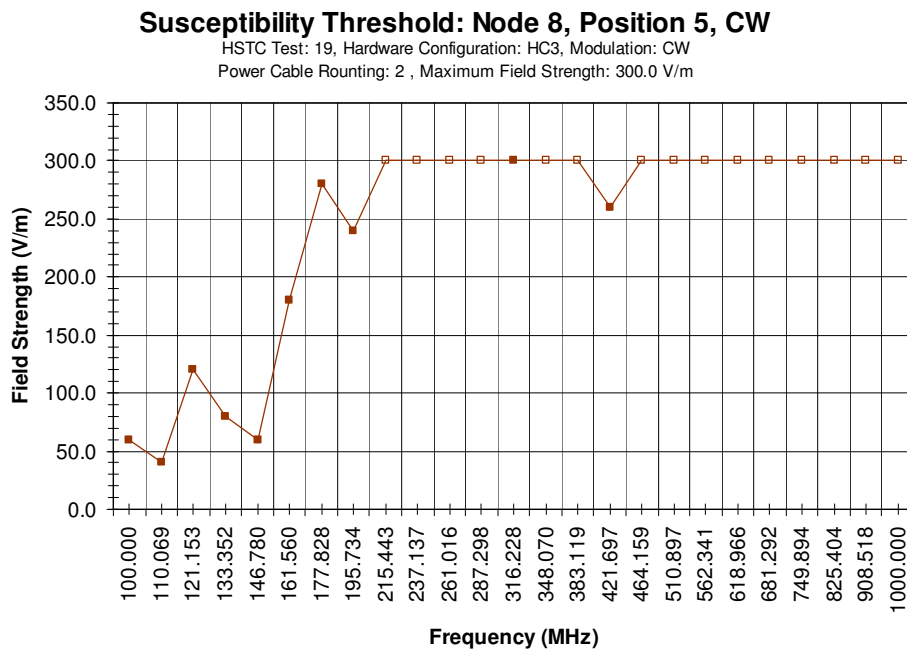


Figure A.19: Measured susceptibility profile for HSTC Test 19

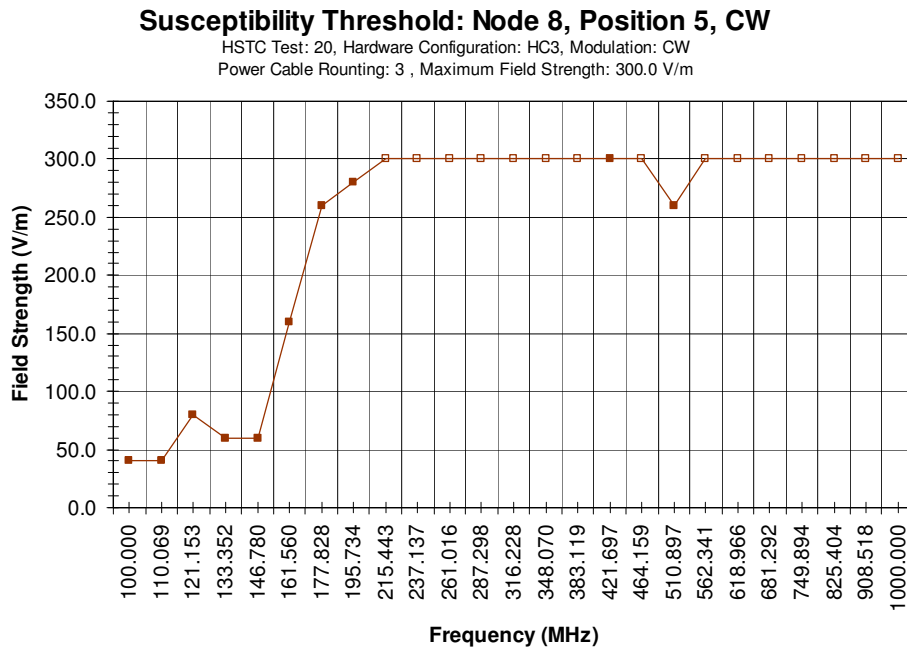


Figure A.20: Measured susceptibility profile for HSTC Test 20

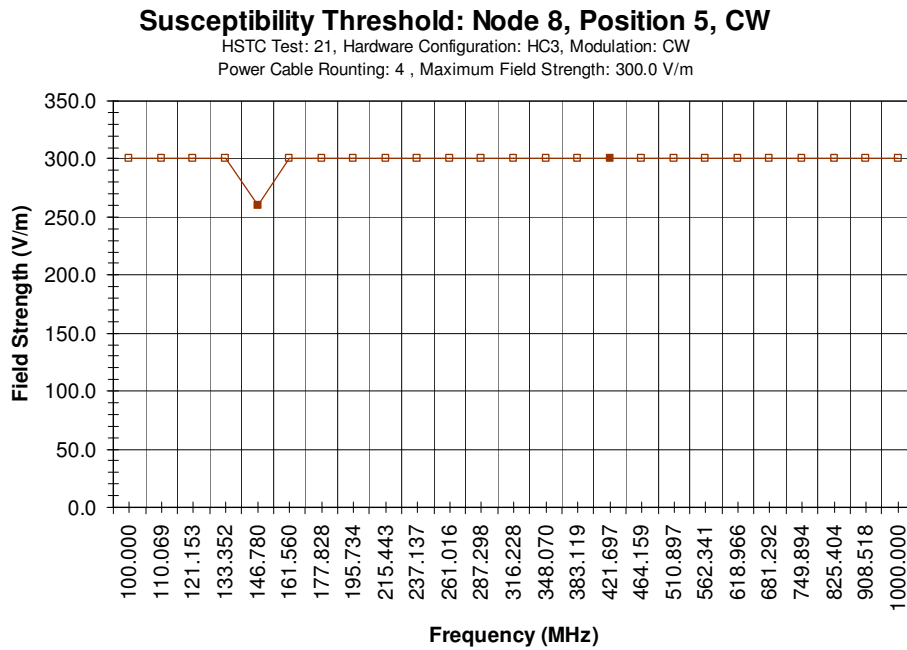


Figure A.21: Measured susceptibility profile for HSTC Test 21

Susceptibility Threshold: Node 7, Position 5, CW

HSTC Test: 22, Hardware Configuration: HC3, Modulation: CW
Power Cable Routing: 2, Maximum Field Strength: 300.0 V/m

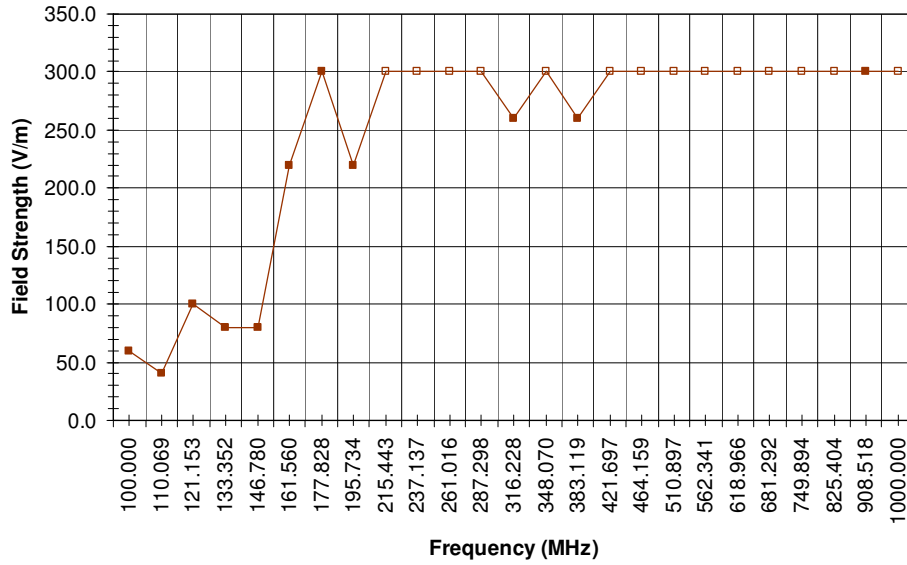


Figure A.22: Measured susceptibility profile for HSTC Test 22

References

- [1] Torres-Pomales, W.; et al: *Plan for the Characterization of HIRF Effects on a Fault-Tolerant Computer Communication System*. NASA-TM-2008-215306, May 2008.
- [2] Torres-Pomales, W.; et al: *Design of Test Articles and Monitoring System for the Characterization of HIRF Effects on a Fault-Tolerant Computer Communication Systems*. NASA-TM-2008-215322, July 2008.
- [3] <http://shemesh.larc.nasa.gov/fm/spider/>
- [4] Ramaker, R.; Krug, W.; and Phebus, W.; *Application of a Civil Integrated Modular Architecture to Military Transport Aircraft*. 26th Digital Avionics Systems Conference (DASC '07), October 21-25, 2007, pp. 2.A.4-1 - 2.A.4.10.
- [5] Yeh, Y. C.: *Design considerations in Boeing 777 fly-by-wire computers*. The 3rd IEEE International Symposium on High-Assurance Systems Engineering (HASE '98), 1998, p. 64.
- [6] Yeh, Y. C.: *Safety Critical Avionics for the 777 Primary Flight Controls System*. 20th Digital Avionics Systems Conference (DASC '01), October 14 – 18, 2001, pp. 1C2/1 - 1C2/11 vol.1.
- [7] Yeh, Y. C.: *Triple-Triple Redundant 777 Primary Flight Computer*. 1996 IEEE Aerospace Applications Conference, volume 1, 1996, pp. 293 - 307.
- [8] Kopetz, Hermann. *Real-Time Systems: Design Principles for Distributed Embedded Applications*. 2nd Edition, Springer, 2011.
- [9] Driscoll, Kevin, et al.: *Data Network Criteria Evaluation Report*. Federal Aviation Administration, DOT/FAA/AR-09/27, July 2009.
- [10] Fuller, Gerald L.: *Understanding HIRF – High Intensity Radiated Fields*. Aviation Communications, Inc., Leesburg, VA, 1995, p. 7-2.
- [11] Hess, Richard: *Computing Platform Architectures for Robust Operation in the Presence of Lightning and Other Electromagnetic Threats*. 16th Digital Avionics Systems Conference (DASC), 1997.
- [12] Arlat, Jean; et al: *Comparison of Physical and Software-implemented Fault Injection Techniques*. IEEE Transaction on Computers, Vol. 52, No. 9, September 2003, pp- 1115 - 1133.
- [13] Karlsson, J.; et al: *Application of Three Physical Fault Injection Techniques to the Experimental Assessment of the MARS Architecture*. Proc. 5th IFIP Working Conference on Dependable Computing for Critical Applications (DCCA-5), IEEE Computer Society Press, Urbana-Champaign, IL, USA, September 1995, pp. 267 - 287.
- [14] Belcastro, Celeste M.: *Laboratory Test Methodology for Evaluating the Effects of Electromagnetic Disturbances on Fault-Tolerant Control Systems*. NASA Technical Memorandum 101665, November 1989.
- [15] Torres-Pomales, Wilfredo; et al: *ROBUS-2: A Fault-Tolerant Broadcast Communication System*. NASA/TM-2005-213540, March 2005.

- [16] Torres-Pomales, Wilfredo; et al: *Design of the Protocol Processor for the ROBUS-2 Communication System*. NASA/TM-2005-213934, November 2005.
- [17] Perry, Douglas: *VHDL*. Third Edition, McGraw-Hill, 1998.
- [18] <http://opensource.arc.nasa.gov/project/robus-2/>
- [19] Wang, Rui; Gray, W. Steve; and González, Oscar R.: *Experimental Validation of a Performance Model for a Distributed Recoverable Boeing 747 Flight Control System Subject to Digital Upsets*. Proceedings of the 43rd IEEE Southeastern Symposium on System Theory, Auburn, Alabama, 2011, pp. 13 - 19.
- [20] Yates, A.M.; et al: *Design of a High-Intensity Radiated Field Fault Injection Experiment for a Fault-Tolerant Distributed Computation and Communication System*. Proceedings of the 2010 Digital Avionics Systems Conference, Salt Lake City, Utah, 2010, pp. 4.E.3-1 - 15.
- [21] Torres-Pomales, Wilfredo; Yates, Amy M.; and Malekpour, Mahyar R.: *Fault Injection and Monitoring Capability for a Fault-Tolerant Distributed Computation System*. NASA/TM-2010-216834, August 2010.
- [22] RTCA DO-160D, Change No. 1, *Environmental Conditions and Test Procedures for Airborne Equipment, Section 20, Radio Frequency Susceptibility (Radiated and Conducted)*, December 2000.
- [23] Ely, Jay J.; Nguyen, Truong X.; and Scarce, Stephen A.: *The Influence of Modulated Signal Risetime in Flight Electronics Radiated Immunity Testing with Mode-Stirred Chamber*. NASA/TM-2000-209844, January 2000.

Acronyms

AC	Alternating Current
ASIC	Application Specific Integrated Circuit
ASCII	American Standard Code for Information Interchange
BIU	Bus Interface Unit
CCP	Controller Coordination Protocol
COTS	Commercial Off-The-Shelf
CPU	Central Processing Unit
CW	Continuous Wave
DC	Direct Current
DSI	Derivation Systems, Inc.
EM	Electromagnetic
EMI	Electromagnetic Interference
FHSTC	Fine HIRF Susceptibility Threshold Characterization
FPGA	Field Programmable Gate Array
FSM	Finite State Machine
HC	Hardware Configuration
HEC	HIRF Effects Characterization
HFA	Hub Fault Analyzer
HIRF	High Intensity Radiated Field
HSTC	HIRF Susceptibility Threshold Characterization
IVHM	Integrated Vehicle Health Management
LUF	Lowest Usable Frequency
Mbps	Mega-bits per second
NFA	Node Fault Analyzer
NIST	National Institute of Standards and Technology
PE	Processing Element
RC	Reverberation Chamber
RF	Radio Frequency
RMU	Redundancy Management Unit
ROBUS	Robust Bus
RPP	ROBUS Protocol Processor
RSPP	Reconfigurable SPIDER Prototyping Platform
RTCA	Radio Technical Commission for Aeronautics
SBIR	Small Business Innovation Research
SHM	System Health Monitor
SIM	Stirrer Induced Modulation
SPIDER	Scalable Processor-Independent Design for Extended Reliability
SUT	System Under Test
TCS	Test Control System
TDMA	Time Division Multiple Access
VHDL	VHSIC Hardware Description Language
VHSIC	Very High Speed Integrated Circuit

REPORT DOCUMENTATION PAGE

*Form Approved
OMB No. 0704-0188*

The public reporting burden for this collection of information is estimated to average 1 hour per response, including the time for reviewing instructions, searching existing data sources, gathering and maintaining the data needed, and completing and reviewing the collection of information. Send comments regarding this burden estimate or any other aspect of this collection of information, including suggestions for reducing this burden, to Department of Defense, Washington Headquarters Services, Directorate for Information Operations and Reports (0704-0188), 1215 Jefferson Davis Highway, Suite 1204, Arlington, VA 22202-4302. Respondents should be aware that notwithstanding any other provision of law, no person shall be subject to any penalty for failing to comply with a collection of information if it does not display a currently valid OMB control number.
PLEASE DO NOT RETURN YOUR FORM TO THE ABOVE ADDRESS.

1. REPORT DATE (DD-MM-YYYY) 01-08-2012		2. REPORT TYPE Technical Memorandum		3. DATES COVERED (From - To)	
4. TITLE AND SUBTITLE Characterization of HIRF Susceptibility Threshold for a Prototype Implementation of an Onboard Data Network				5a. CONTRACT NUMBER	
				5b. GRANT NUMBER	
				5c. PROGRAM ELEMENT NUMBER	
				5d. PROJECT NUMBER	
6. AUTHOR(S) Torres-Pomales, Wilfredo				5e. TASK NUMBER	
				5f. WORK UNIT NUMBER 534723.02.02.07.30	
				8. PERFORMING ORGANIZATION REPORT NUMBER L-20157	
7. PERFORMING ORGANIZATION NAME(S) AND ADDRESS(ES) NASA Langley Research Center Hampton, VA 23681-2199				10. SPONSOR/MONITOR'S ACRONYM(S) NASA	
9. SPONSORING/MONITORING AGENCY NAME(S) AND ADDRESS(ES) National Aeronautics and Space Administration Washington, DC 20546-0001				11. SPONSOR/MONITOR'S REPORT NUMBER(S) NASA/TM-2012-217754	
12. DISTRIBUTION/AVAILABILITY STATEMENT Unclassified - Unlimited Subject Category 60 Availability: NASA CASI (443) 757-5802					
13. SUPPLEMENTARY NOTES					
14. ABSTRACT An experiment was conducted to characterize the effects of HIRF-induced upsets on a prototype onboard data network. The experiment was conducted at the NASA Langley Research Center's High Intensity Radiation Field Laboratory and used a generic distributed system prototyping platform to realize the data network. This report presents the results of the hardware susceptibility threshold characterization which examined the dependence of measured susceptibility on factors like the frequency and modulation of the radiation, layout of the physical nodes and position of the nodes in the test chamber. The report also includes lessons learned during the development and execution of the experiment.					
15. SUBJECT TERMS Avionics; Data network; High-intensity electromagnetic field; Resilience; Safety					
16. SECURITY CLASSIFICATION OF:			17. LIMITATION OF ABSTRACT	18. NUMBER OF PAGES	19a. NAME OF RESPONSIBLE PERSON
a. REPORT	b. ABSTRACT	c. THIS PAGE			STI Help Desk (email: help@sti.nasa.gov)
U	U	U	UU	47	19b. TELEPHONE NUMBER (Include area code) (443) 757-5802